Role of the Chromosome Architectural Factor SMCHD1 in X-Chromosome Inactivation, Gene Regulation, and Disease in Humans

Chen-Yu Wang,[*,†] Harrison Brand,[‡,§,,††] Natalie D. Shaw,[‡‡,§§] Michael E. Talkowski,[‡,§,**,††] and Jeannie T. Lee[*,†,1]**

[*]Department of Molecular Biology, [††]Center for Human Genetic Research, and [‡‡]Department of Medicine, Massachusetts General Hospital, Boston, Massachusetts 02114, [†]Department of Genetics, Harvard Medical School, Boston, Massachusetts 02115, [‡]Department of Neurology, Massachusetts General Hospital and Harvard Medical School, Boston, Massachusetts 02114, [§]Program in Medical and Population Genetics and [**]Center for Mendelian Genomics, Broad Institute of MIT and Harvard, Cambridge, Massachusetts 02142, [§§]National Institute of Environmental Health Sciences, Research Triangle Park, North Carolina 27709

ORCID IDs: 0000-0002-3912-5113 (C.-Y.W.); 0000-0001-7786-8850 (J.T.L.)

ABSTRACT Structural maintenance of chromosomes flexible hinge domain-containing 1 (SMCHD1) is an architectural factor critical for X-chromosome inactivation (XCI) and the repression of select autosomal gene clusters. In mice, homozygous nonsense mutations in *Smchd1* cause female-specific embryonic lethality due to an XCI defect. However, although human mutations in *SMCHD1* are associated with congenital arhinia and facioscapulohumeral muscular dystrophy type 2 (FSHD2), the diseases do not show a sex-specific bias, despite the essential nature of XCI in humans. To investigate whether there is a dosage imbalance for the sex chromosomes, we here analyze transcriptomic data from arhinia and FSHD2 patient blood and muscle cells. We find that *X*-linked dosage compensation is maintained in these patients. In mice, SMCHD1 controls not only protocadherin (*Pcdh*) gene clusters, but also *Hox* genes critical for craniofacial development. Ablating *Smchd1* results in aberrant expression of these genes, coinciding with altered chromatin states and three-dimensional (3D) topological organization. In a subset of FSHD2 and arhinia patients, we also found dysregulation of clustered *PCDH*, but not *HOX* genes. Overall, our study demonstrates preservation of XCI in arhinia and FSHD2, and implicates SMCHD1 in the regulation of the 3D organization of select autosomal gene clusters.

KEYWORDS SMCHD1; X-chromosome inactivation; *HOX* genes; clustered protocadherin genes; epigenetics; chromatin

X-CHROMOSOME inactivation (XCI) silences gene expression on one of the two *X* chromosomes in female mammals, thereby ensuring balanced dosage of *X*-linked genes between *XY* males and *XX* females (Starmer and Magnuson 2009; Lee 2011; Wutz 2011; Disteche 2012; Mira-Bontenbal and Gribnau 2016). Aberrant dosage of even a fraction of *X*-linked genes in humans can produce an abnormal phenotype, as exemplified by Turner (*XO*) and Klinefelter (*XXY*) syndromes. In mice, perturbation of XCI in early development has devastating consequences: deletion of *Xist* (*X*-inactive-specific transcript), the master regulator of XCI (Brockdorff *et al.* 1991; Brown *et al.* 1991), causes female-specific embryonic lethality early in gestation around the time of normal XCI initiation (Marahrens *et al.* 1997; Yang *et al.* 2016).

A mutagenesis screen in mice previously identified *Smchd1* as a locus essential for transgene silencing and female embryonic development (Blewitt *et al.* 2005, 2008). *Smchd1* encodes structural maintenance of chromosomes (SMC) flexible hinge domain-containing 1 (SMCHD1), a 230-kDa protein with an N-terminal GHKL (Gyras, Hsp90, Histidine Kinase, MutL)-type ATPase domain and a C-terminal SMC hinge domain that mediates SMCHD1 homodimerization (Blewitt *et al.* 2008; Brideau *et al.* 2015; Chen *et al.* 2015, 2016). Several studies have now demonstrated its unequivocal role in XCI (Blewitt *et al.* 2005, 2008; Gendrel *et al.* 2012, 2013; Mould *et al.* 2013;

doi: https://doi.org/10.1534/genetics.119.302600
Manuscript received May 7, 2019; accepted for publication August 13, 2019; published Early Online August 16, 2019.
Supplemental material available at FigShare: https://doi.org/10.25386/genetics.9633668.
[1]Corresponding author: Department of Molecular Biology, Simches Research Center, CPZN 6.624, 185 Cambridge St., Boston, MA 02139. E-mail: lee@molbio.mgh.harvard.edu

Nozawa *et al.* 2013; Jansz *et al.* 2018a,b; Sakakibara *et al.* 2018; Wang *et al.* 2018; Gdula *et al.* 2019). Indeed, SMCHD1 is enriched on the inactive *X* chromosome (Xi) (Blewitt *et al.* 2008), but is apparently recruited to the Xi relatively late during XCI in an *ex vivo* female embryonic stem (ES) cell model (Gendrel *et al.* 2012). In contrast to *Xist* mutants, female mice null for *Smchd1* do not perish during the peri-implantation stage, but rather only in midgestation [by embryonic day (E)11.5] (Blewitt *et al.* 2005, 2008). Thus, SMCHD1 is thought to act later during the XCI cascade. Indeed, recent work has shown that SMCHD1 functions in finalizing the three-dimensional (3D) reorganization the Xi, in particular at the level of chromosome compartments (Wang *et al.* 2018, 2019). During XCI, Xist recruits Polycomb Repressive Complex 1 to fuse A/B compartments into "S1/S2" compartments. SMCHD1 then binds S1/S2 structures and merges them to create a compartment-less Xi architecture. Loss of SMCHD1 and a failure to fuse S1/S2 leads to regional defects in Xist spreading and erosion of heterochromatic silencing, coinciding with derepression of 43% of Xi genes in SMCHD1-deficient cells (Wang *et al.* 2018). Thus, SMCHD1 plays a critical role during the progression through XCI.

Importantly, SMCHD1 shows a high degree of sequence similarity between mice and humans (87% protein sequence identity). SMCHD1 also associates with the Xi in both species (Blewitt *et al.* 2008; Nozawa *et al.* 2013). Given the conservation of structure and function across species, *SMCHD1* mutations in humans would be expected to cause defective XCI and possibly female-specific phenotypes. A review of the human Genome Aggregation Database (gnomAD) of nearly 140,000 control exomes and whole genomes reveals that *SMCHD1* is strongly depleted for loss-of-function (LoF) mutations (probability of being loss of function intolerant (pLI) = 1; observed/expected constraint metric (o/e) = 0.09), and that there is complete absence of individuals with homozygous LoF variants. These data suggest that a complete loss of SMCHD1 activity may be incompatible with life in either sex.

Human genetic studies over the last few years have now established a diverse phenotypic spectrum of complex disorders associated with *SMCHD1* mutations. It was previously established that missense and LoF mutations in *SMCHD1* are a necessary but insufficient component of a complex oligogenic mechanism associated with facioscapulohumeral muscular dystrophy type 2 (FSHD2) (Lemmers *et al.* 2012; Sacconi *et al.* 2013), a late-onset, slowly progressive muscle disease. *SMCHD1* mutations also serve as a genetic modifier of disease severity in FSHD type 1 (Sacconi *et al.* 2013). Surprisingly, it has been recently demonstrated that some of these same FSHD2 mutations, and other missense variants of *SMCHD1*, contribute to a rare craniofacial malformation that involves the complete absence of an external nose, known as congenital arhinia (Gordon *et al.* 2017; Shaw *et al.* 2017). While FSHD2 and arhinia-associated mutations are only found in the heterozygous state in humans, heterozygous mutations can be equally or more detrimental than null mutations, either through haploinsufficiency or a dominant-negative mechanism (for instance, interference with SMCHD1 homodimerization) (Wilkie 2017). Indeed, several studies suggest that the phenotypes associated with arhinia and FSHD2 likely arise from either a haploinsufficiency or a dominant-negative effect (Lemmers *et al.* 2012, 2015; Shaw *et al.* 2017; de Greef *et al.* 2018).

An intriguing aspect of these disorders is that none exhibits a sex bias, despite the established role of SMCHD1 in XCI. Could SMCHD1 dysfunction cause severe disease without simultaneously impacting XCI? Furthermore, if the SMCHD1 mutations did affect XCI, could XCI defects contribute to the presentation of arhinia and FSHD2? Here, we explore the genotype–phenotype relationships by analyzing transcriptomic data from human arhinia and FSHD2 patients, and document a surprising lack of XCI defects. However, we identify a link between SMCHD1 dysfunction and misregulation of select autosomal gene clusters that are candidate downstream targets for SMCHD1-related disorders.

Materials and Methods

RNA-sequencing analysis

RNA-sequencing (RNA-seq) data of female/male mouse embryonic stem (ES) cells (mESCs) (GSE54016) (Gendrel *et al.* 2014), female/male mouse liver cells (GSE48109) (Sugathan and Waxman 2013), male wild-type (WT)/*Smchd1*$^{MommeD1/MommeD1}$ (*Smchd1*$^{-/-}$) mouse neural stem/progenitor cells (NPCs) (GSE65747) (Chen *et al.* 2015), female WT/*Smchd1*$^{-/-}$ mouse NPCs (GSE99991) (Wang *et al.* 2018), and FSHD2 patients (GSE56787) (Yao *et al.* 2014) were downloaded from the Gene Expression Omnibus (GEO). Arhinia patient RNA-seq data have been published (Shaw *et al.* 2017). Reads were aligned to mm9 or hg19 using TopHat2 (Kim *et al.* 2013), with PCR duplicates removed from paired-end data sets. Strand information was resolved if the library was constructed using strand-specific protocols. Uniquely mapped exonic reads were counted using Homer (Heinz *et al.* 2010), and fragments per kilobase of transcript per million mapped reads (FPKMs)/reads per kilobase of transcript per million mapped reads (RPKMs) were calculated by dividing the RNA-seq exonic fragment/read count of each gene by the length of exons (kilobases) and total mapped exonic fragments/reads (million). Fold changes were calculated by dividing the FPKM/RPKMs of samples with *SMCHD1* mutations with those of controls. To compare the fold changes of autosomal and *X*-linked genes, only genes with FPKM/RPKM > 0.1 were included. The lists of class I SMCHD1-senstive genes and genes subject to XCI in female mouse NPCs have been reported (Wang *et al.* 2018). To identify "facultative escapees," we first compiled a list of all escapees reported from previous studies (Yang *et al.* 2010; Lopes *et al.* 2011; Splinter *et al.* 2011; Calabrese *et al.* 2012; Li *et al.* 2012; Pinter *et al.* 2012; Berletch *et al.* 2015; Marks *et al.* 2015) and defined facultative escapees as reported escapees that do not belong to "constitutive escapees" defined in female mouse NPCs (Wang *et al.* 2018). The human homologs of class I SMCHD1-senstive

genes were identified based on a list of human–mouse homologs retrieved from the Mouse Genome Informatics database. We defined constitutive escapees ("E" or "Mostly E"), facultative escapees ("VE" or "Mostly VE"), and genes subject to XCI ("S" or "Mostly S") in humans based on a previous study (Balaton *et al.* 2015), which comprehensively classified the XCI status of *X*-linked genes by compiling several existing studies. In the FSHD RNA-seq data sets, we excluded data of a control individual (C6) from our analyses as the library was sequenced at a much lower depth. Cumulative distribution plots were constructed using R and ggplot2. *P*-values were computed by Wilcoxon ranked sum test (unpaired, one-sided) using R. To visualize RNA-seq coverage, we generated *f*ragment-*p*er-*m*illion (fpm)-normalized bigWig files, which were displayed using Integrative Genomics Viewer (IGV) with scales indicated in each track.

To identify differentially expressed autosomal genes in *Smchd1*$^{-/-}$ female mouse NPCs, we analyzed RNA-seq data sets of two WT and two *Smchd1*$^{-/-}$ clones that carry two *X* chromosomes, together with those of one WT and one *Smchd1*$^{-/-}$ clone with *X*O genotypes, using the DESeq tool (Anders and Huber 2010). The inclusion of additional clones led to a reduced number of differentially expressed genes than that reported previously (Wang *et al.* 2018), as there was variation in gene expression between clones. Functional annotation clustering was performed using the Database for Annotation, Visualization and Integrative Discovery (DAVID) (Huang da *et al.* 2009), with stringency set as "medium." Gene Ontology (GO) analysis was also performed using DAVID (Huang da *et al.* 2009). For functional annotation clustering and GO analysis, *P*-values corrected by the Benjamini–Hochberg method were presented.

To perform DESeq analyses for arhinia patients Y1 and B1, we compared each patient with 10 controls (A2, AE2, AE3, AE4, AH2, AH4, AH6, D2, D3, and D4). To perform DESeq analysis for FSHD2 patient F14, we compared F14 with eight controls (C1, C2, C3, C4, C5, C7, C8, and C9).

Chromatin immunoprecipitation-sequencing and in situ Hi-C data analysis

H3K4me3, H3K27me3, CCCTC-binding factor (CTCF), and RAD21 chromatin immunoprecipitation-sequencing (ChIP-seq) and *in situ* Hi-C data in mouse NPCs, derived by *in vitro* differentiation of WT and *Smchd1*$^{-/-}$ mESCs, were available from the GEO (GSE99991). EZH2 ChIP-seq data in mouse NPCs were uploaded to GSE126257. We displayed fpm-normalized ChIP-seq coverage "comp" (compiling allele-specific and nonallelic reads) tracks using IGV, with scales indicated in each track. Replicate 1 of ChIP-seq is shown in the figures, but replicate 2 demonstrated similar patterns at the *Pcdh* and *Hox* loci as replicate 1. Two biological replicates of *in situ* Hi-C data were pooled to increase depth. Combined Hi-C summary files were converted to .hic files, which were then displayed by Juicebox using the "balanced" mode for normalization (Durand *et al.* 2016), with resolutions and scales indicated in each panel. WT/*Smchd1*$^{-/-}$ maps were also computed by Juicebox. The hic files have been uploaded to the GEO (GSE126257).

Data availability

All next-generation sequencing data are available at the GEO with the accession numbers GSE54016, GSE48109, GSE65747, GSE99991, GSE56787, and GSE126257. Supplemental material available at FigShare: https://doi.org/10.25386/genetics.9633668.

Results

Dosage compensation is preserved in female arhinia and FSHD2 patients

To determine if heterozygous mutations in *SMCHD1* identified in patients with arhinia or FSHD2 are accompanied by defective XCI, we analyzed published RNA-seq data sets in lymphoblastoid cell lines (LCLs) from four female arhinia patients, myogenic cells from two female FSHD2 patients (Figure 1, A and B), and corresponding cell types from female controls. Arhinia patients carry heterozygous missense *SMCHD1* mutations that are clustered at the N-terminal ATPase domain of the protein (Gordon *et al.* 2017; Shaw *et al.* 2017), whereas FSHD2 patients harbor missense, nonsense, and deletion mutations spanning the entire *SMCHD1* locus (Figure 1, A and B) (Lemmers *et al.* 2012; Jansz *et al.* 2017; Shaw *et al.* 2017). The interrogation of individual *X*-linked genes with this small sample size and limited number of replicates posed a challenge because defective XCI typically leads to upregulation of any given *X*-linked gene by only up to twofold (Gendrel *et al.* 2012; Mould *et al.* 2013; Yang *et al.* 2016; Wang *et al.* 2018). To overcome this technical limitation, we compared the cumulative distribution of the fold change of *X*-linked genes relative to all autosomal genes in female patients and controls (Yang *et al.* 2016; Carrette *et al.* 2018), reasoning that even a small degree of upregulation of many *X*-linked genes would cause a significant deviation in the *X*-linked gene fold change distribution compared with the distribution for autosomal genes.

To validate the sensitivity and specificity of our analytical pipeline for detecting dosage imbalances, we ran the analysis on mouse cells for which a dosage imbalance has been established. First, we examined publicly available RNA-seq data from *XX* and *XY* mESCs (Gendrel *et al.* 2014). Undifferentiated female mESCs have two active *X* chromosomes (Xa), whereas male mESCs have one Xa. Indeed, we observed a rightward shift of *X*-linked fold change distribution relative to autosomes between female and male mESCs (Figure 1C, left), indicating disproportionate upregulation of *X*-linked genes relative to autosomes in females. This "*X*–A imbalance" was absent, as expected, between WT male and female mouse hepatocytes (Sugathan and Waxman 2013), as these fully differentiated cells had undergone XCI. (Figure 1C, left center). We also observed *X*–A imbalance in *Smchd1*$^{-/-}$ NPCs derived from female mESCs

A

Disease	Patient ID	Mutation type	Nucleotide mutation	Exon	Amino acid alteration	Position	SMCHD1 abundance	SMCHD1 activity
Arhinia	A1	Missense	g.2667021A>C	3	p.Asn139His	GHKL ATPase	No effect (Shaw et al, 2017)	Not tested
	AG1	Missense	g.2667016G>A	3	p.Gly137Glu	GHKL ATPase	No effect (Shaw et al, 2017)	Increased ATPase activity (Gurzau et al., 2018)
	AH1	Missense	g.2687896A>T	10	p.Gly400Leu	Extended region	No effect (Shaw et al, 2017)	Not tested
	Y1	Missense	g.2667021A>C	3	p.Asn139His	GHKL ATPase	No effect (Shaw et al, 2017)	Not tested
FSHD2	F14	Missense	g.2763729T>C	37	p.Phe1554Ser	Linker region	Not tested	Not tested
	F20	Deletion	g.2697999_2698003del	10	p.Tyr434*	Extended region	Not tested	Not tested

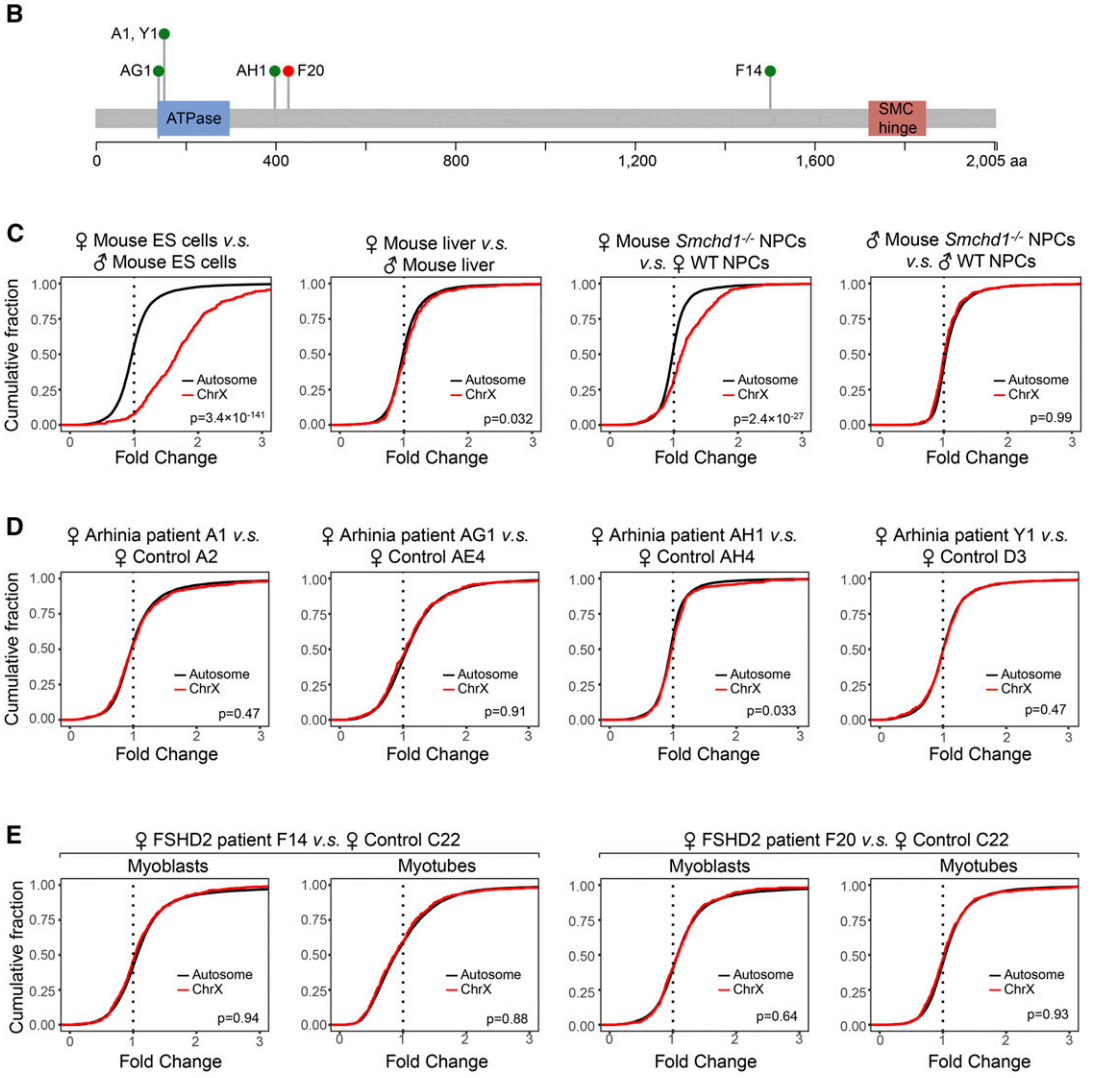

Figure 1 Dosage compensation is preserved in female arhinia and FSHD2 patients harboring *SMCHD1* mutations. (A) A table listing the cohort of female arhinia and FSHD2 patients, and their associated *SMCHD1* mutations included in this study. Arhinia patients harboring *SMCHD1* mutations often exhibit normal levels of SMCHD1 protein (Shaw *et al.* 2017). In contrast, it has been reported that *SMCHD1* mutations in FSHD2 patients are usually associated with reduced SMCHD1 protein levels (Lemmers *et al.* 2012), although the two FSHD2 patients listed here have not been tested for SMCHD1 levels. (B) The domain structure of human SMCHD1 protein with the locations of mutations found in patients listed in (A) overlaid. Green dots, missense mutations. Red dot, nonsense or frameshift mutations. This figure was modified from Shaw *et al.* (2017). (C) CDPs for fold changes of *X*-linked and autosomal genes in mouse cells. Note that *X*–A imbalance was not seen in male *Smchd1*$^{-/-}$ mouse NPCs, indicating that *X*–A imbalance in *Smchd1*$^{-/-}$ females originated from the inactive *X* chromosome. *P*-values given by Wilcoxon ranked sum test (unpaired, one-sided). (D) CDPs for fold changes of *X*-linked and autosomal genes in female arhinia patients *vs.* female controls. (E) CDPs for fold changes of *X*-linked and autosomal genes in female FSHD2 patients *vs.* female controls. CDP, cumulative distribution plot; Chr, chromosome; ES, embryonic stem; FSHD2, facioscapulohumeral muscular dystrophy type 2; ID, identifier; NPC, neural progenitor cell; SMC, structural maintenance of chromosomes; SMCHD1, SMC flexible hinge domain-containing 1; GHKL, Gyras, Hsp90, Histidine Kinase, MutL; WT, wild-type.

(Figure 1C, right center) (Wang *et al.* 2018) but not male mice (Figure 1C, right) (Chen *et al.* 2016). These analyses demonstrate the robustness of our analytical pipeline.

We next examined RNA-seq data from female arhinia and FSHD2 patients. We analyzed each patient separately, reasoning that each female patient harbors a distinct mutation that may affect SMCHD1 differently (Figure 1A). Indeed, recent work has shown varying ATPase activity levels in distinct *SMCHD1* mutants (Gurzau *et al.* 2018). Examining each patient separately, we found that none of the four female arhinia patients with heterozygous missense mutations in *SMCHD1* demonstrated *X*–A imbalance (Figure 1D). Interestingly, *X* upregulation was also not detected in either female FSHD2 patient (Figure 1E), despite one of them (F20) harboring a frameshifting deletion in *SMCHD1*. Thus, these specific *SMCHD1* mutations do not cause dosage compensation defects, at least when examined on a global chromosomal scale in heterozygous human patients.

Class I genes resist arhinia- and FSHD2-associated SMCHD1 mutations

Previous studies showed that in mice, SMCHD1 is required to silence a specific subset of genes on the Xi, referred to as class I SMCHD1-sensitive genes (class I genes, $n = 126$) (Wang *et al.* 2018). In the absence of SMCHD1, class I genes exhibited local Xist RNA-spreading defects and erosion of heterochromatic silencing, while other genes on the Xi were not affected. Overall, *Smchd1* ablation leads to defective silencing in $\leq$ 43% of genes normally subject to XCI (Gendrel *et al.* 2013; Mould *et al.* 2013; Wang *et al.* 2018). Indeed, the *X*–A imbalance between *Smchd1*$^{-/-}$ and WT mouse NPCs was weaker than that between female and male mESCs (compare Figure 1C, left and right center), indicating a partial XCI defect. We reasoned that an *X*–A imbalance in these patients may not be evident if only a small fraction of *X*-linked genes were dysregulated. To address this possibility, we tested if a weaker *X*–A imbalance could be detected in patients by focusing on the subset of genes that are known to be dependent on SMCHD1 for silencing.

To validate the approach, we first compared the expression of "escapees," a subset of *X*-linked genes resistant to XCI, between female and male controls (Supplemental Material, Figure S1). We focused on constitutive escapees, which resist XCI in all cells (Berletch *et al.* 2011; Balaton and Brown 2016). When examining fold change distribution upon aggregating all *X*-linked genes, the increased dosage of constitutive escapees in females led to a minimal *X*–A imbalance between females and males (Figure S1A), which was not seen between same-sex individuals (Figure S1, B and C). Notably, when analyzing constitutive escapees ($n = 49$) separately from other *X*-linked genes, we detected upregulation of these escapees in females relative to males (Figure S1D), but not between individuals of the same sex (Figure S1, E and F). Thus, *X*–A imbalance can be sensitively detected by examining select *X*-linked genes with increased dosage.

We next focused analyses on human *X*-linked genes homologous to mouse class I genes ($n = 116$). Significantly, female arhinia patients ($n = 4$) and FSHD2 patients ($n = 2$) did not demonstrate upregulation of class I genes compared to female controls (Figure 2, B and C). In mice, the unique dependence of class I genes on SMCHD1 for silencing is intriguing. Because SMCHD1 binds broadly along the entire Xi in mice (Wang *et al.* 2018), the specific effect on class I genes cannot be conferred by region-specific SMCHD1 binding. We asked if geographic characters on the Xi may affect regional SMCHD1 sensitivity. It has been reported that class I genes form clusters (Gendrel *et al.* 2013; Wang *et al.* 2018). Interestingly, class I gene clusters overlapped with regions known to be rich in facultative escapees ($r = 0.64$) (Figure 3, A and B), a distinct subset of escapees that resist XCI only in select cells or tissues (Berletch *et al.* 2011; Balaton and Brown 2016) (Table S1). Furthermore, facultative escapees were selectively enriched in class I genes ($P < 0.0001$) (Figure 3C), and nonescaping class I genes tended to be in the vicinity of escapees (Figure 3, D and E), suggesting that regions harboring facultative escapees may be more sensitive to *Smcdh1* dysfunction. Indeed, facultative escapees were upregulated in *Smchd1*$^{-/-}$ female mouse NPCs (Figure 4A). Our findings in mice are in line with a study that links genetic variants of *SMCHD1* to facultative escapees in humans (Luijk *et al.* 2018). In spite of this, we observed no upregulation of facultative escapees ($n = 44$) in female arhinia ($n = 4$) or FSHD2 ($n = 2$) patients (Figure 4, B and C). Collectively, these data indicate that arhinia- and FSHD2-assocated *SMCHD1* mutations do not affect dosage compensation of *X*-linked genes when they are in the heterozygous state. Thus, dosage compensation is less sensitive to SMCHD1 dysfunction than are craniofacial development and muscular function.

SMCHD1 controls the epigenetic state and 3D organization of the mouse Pcdh cluster

It is believed that *SMCHD1* mutations, in conjunction with a shortened permissive D4Z4 array, cause FSHD2 via derepression of the leading FSHD candidate gene, *D*ouble *H*omeobox *4* (*DUX4*) (Lemmers *et al.* 2012), but other unknown genetic (or) environmental factors may also be contributory (Jones *et al.* 2012). The molecular basis of arhinia remains unclear, but our previous transcriptome studies suggested *DOK7*, *TGIF1*, *KDM6A*, and *ICK* to be dysregulated in arhinia patients (Shaw *et al.* 2017). To gain insight into the pathogenesis of arhinia and FSHD2, we investigated the effect of SMCHD1 dysfunction on autosomal gene expression. We began with an examination of autosomal genes dysregulated in *Smchd1*$^{-/-}$ mouse cells, reasoning that the stronger effect of homozygous mutations may allow a more targeted approach in analyzing the patient data, where heterozygous mutations may only yield subtle changes in gene expression.

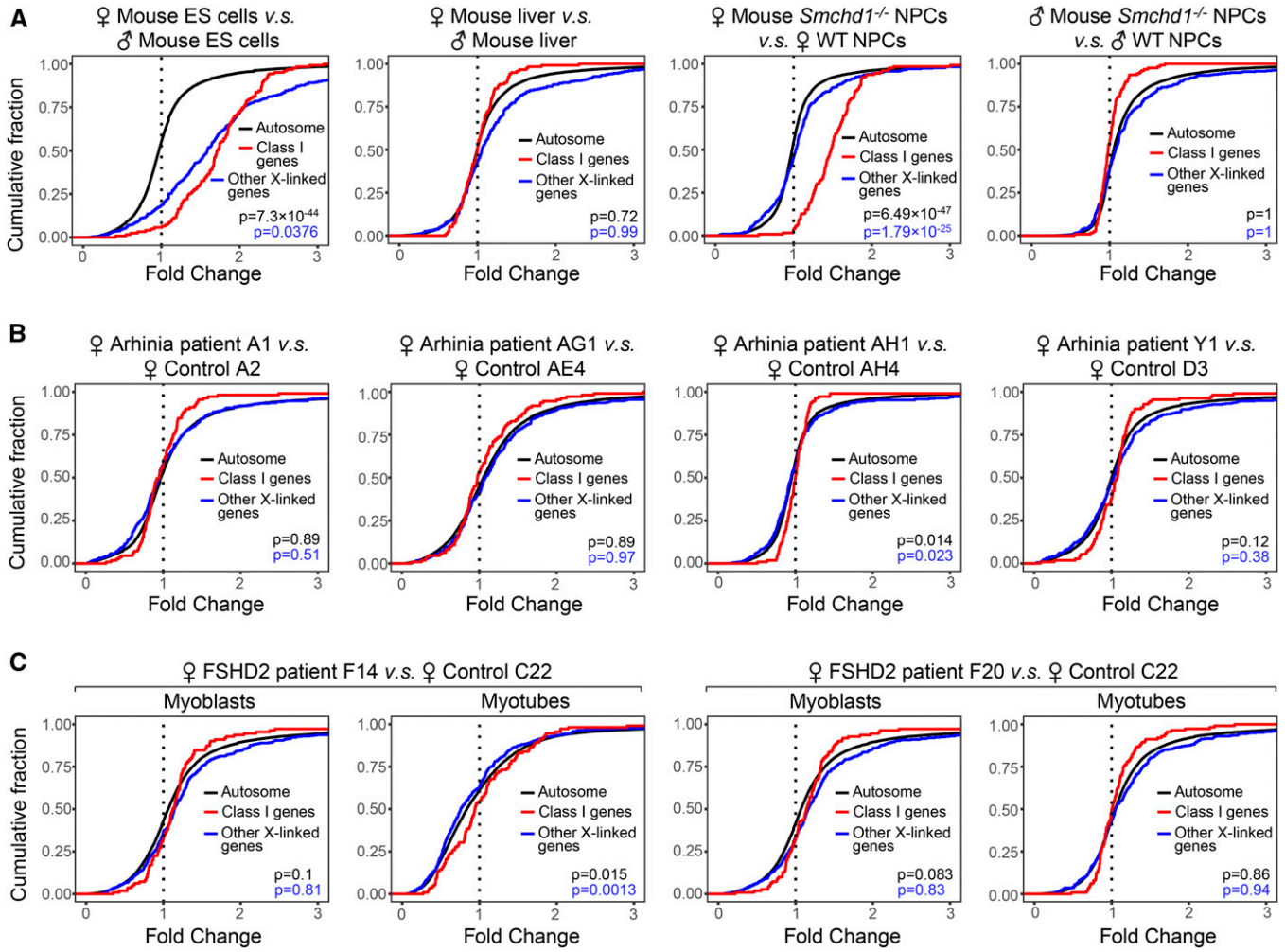

Figure 2 Human homologs of class I SMCHD1-sensitive Xi genes resist upregulation in heterozygous female patients. (A) CDPs comparing class I SMCHD1-sensitive genes (class I genes), other *X*-linked genes, and autosomal genes in mouse cells. *P*-values: class I genes *vs.* autosomal genes (black); class I genes *vs.* other *X*-linked genes (blue). *P*-values given by Wilcoxon ranked sum test (unpaired, one-sided). (B) CDPs comparing human homologs of class I SMCHD1-sensitive genes (class I genes), other *X*-linked genes, and autosomal genes in female arhinia patients *vs.* female controls. (C) CDPs comparing human homologs of class I SMCHD1-sensitive genes (class I genes), other *X*-linked genes, and autosomal genes in female FSHD2 patients *vs.* female controls. CDP, cumulative distribution plot; ES, embryonic stem; FSHD2, facioscapulohumeral muscular dystrophy type 2; NPC, neural progenitor cell; SMCHD1, structural maintenance of chromosomes flexible hinge domain-containing 1; WT, wild-type; Xi, inactive *X* chromosome.

It is known that *Smchd1*$^{-/-}$ mice exhibit upregulation and CpG hypomethylation of the clustered protocadherin (*Pcdh*) genes (Gendrel *et al.* 2012; Mould *et al.* 2013; Chen *et al.* 2015; Wang *et al.* 2018). These genes encode a subgroup of cadherin proteins critical for neuronal diversity and neural circuit formation (Zipursky and Sanes 2010; Chen and Maniatis 2013; Yagi 2013; Mountoufaris *et al.* 2017). The *Pcdh* genes are arranged into three closely linked clusters—α, β, and γ—with dysregulation of the *Pcdha* cluster in the *Smchd1*$^{-/-}$ background being most consistently observed. Each *Pcdha* mRNA contains one of the 14 tandemly arranged "variable exons," with each carrying a promoter, and three "constant exons" shared by all *Pcdha* isoforms (Figure 5A). Through stochastic promoter choice, *Pcdha* isoforms carrying the 12 "alternate" exons exhibit combinatorial and monoallelic expression in neuronal lineages, whereas isoforms carrying the two "C-type" exons are expressed biallelically and constitutively (Wu and Maniatis 1999; Wu *et al.* 2001; Tasic *et al.* 2002; Wang *et al.* 2002; Esumi *et al.* 2005). To probe deeper into how the *Pcdh* genes are aberrantly regulated in the absence of SMCHD1, we reanalyzed published RNA-seq data in WT ($n = 3$) and *Smchd1*$^{-/-}$ ($n = 3$) female mouse NPC clones, which were derived from *in vitro* differentiation of WT and *Smchd1*$^{-/-}$ mESCs (Wang *et al.* 2018). In all three *Smchd1*$^{-/-}$ clones, we observed upregulation of all 14 *Pcdha* isoforms (Figure 5B, left), whereas the expression of *Pcdhb* (Figure 5B, right) and *Pcdhg* clusters (Figure S2A) was similar between WT and *Smchd1*$^{-/-}$ clones. Strand-specific RNA-seq coverage profiles (Figure 5A, "+" strand)

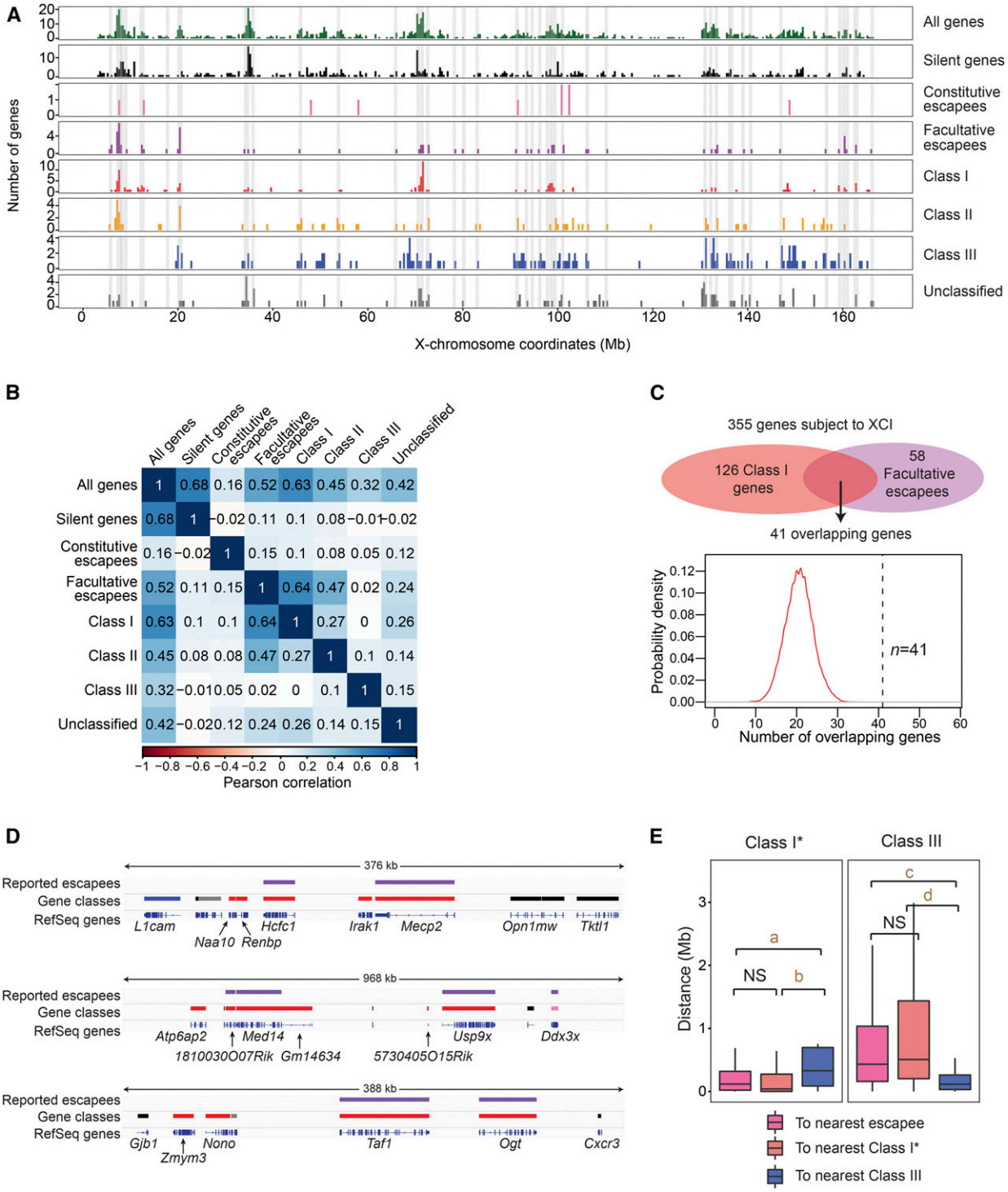

Figure 3 Inactivation of facultative escapees is sensitive to *Smchd1* ablation in mice. (A) Location of facultative escapees relative to various *X*-linked gene classes. Gray-shaded areas are regions with facultative escapees. (B) Pearson correlation analysis of the occurrence of facultative escapees relative to various *X*-linked gene classes on the *X*. (C) Testing the random likelihood of having 41 class I genes as facultative escapees. Random samplings of 126 genes from 355 genes subject to XCI in which 58 are facultative escapees were simulated 10,000 times. A probability density plot was generated for the number of facultative escapees sampled. (D) Representative examples of class I genes that either overlap with or are adjacent to reported escapees. Top track: all reported (constitutive and facultative) escapees (purple bars). Middle track: silent genes (black bars), constitutive escapees (pink bars), class I genes (red bars), unclassified genes (gray bars), and class III genes (blue bars). Bottom track: RefSeq genes. (E) Nearest neighbor analysis: box plots showing distribution of distances of class I and class III genes from each other, and to escapees. *e.g.*, the left panel shows the distance distribution from a class I gene to the nearest escapee (pink), class I (red), or class III (blue) gene. For this analysis, the 41 facultative escapees are removed from the class I list (class I*). *P*-values were determined by Wilcoxon ranked sum test. NS, not significant ($P > 0.05$). a, $P = 3.303 \times 10^{-4}$. b, $P = 3.221 \times 10^{-6}$. c, $P = 6.14 \times 10^{-12}$. d, $P = 8.556 \times 10^{-15}$. XCI, X-chromosome inactivation.

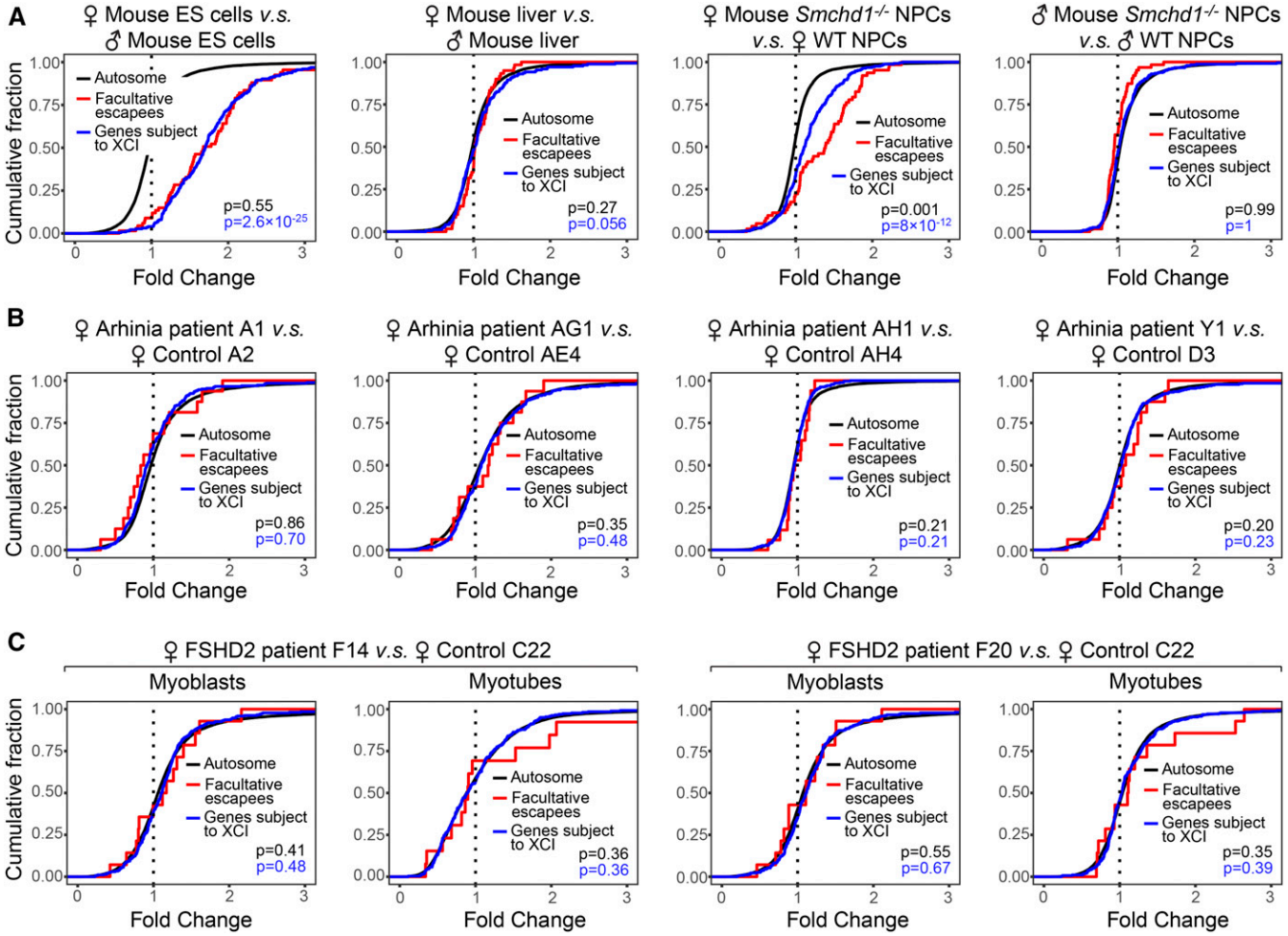

Figure 4 Behavior of facultative escapees in female arhinia and FSHD2 patients. (A) CDPs comparing facultative escapees, genes subject to XCI, and autosomal genes in mouse cells. *P*-values: facultative escapees *vs.* autosomal genes (black); facultative escapees *vs.* genes subject to XCI (blue). *P*-values given by Wilcoxon ranked sum test (unpaired, one-sided). (B) CDPs comparing facultative escapees, genes subject to XCI, and autosomal genes in female arhinia patients *vs.* female controls. (C) CDPs comparing facultative escapees, genes subject to XCI, and autosomal genes in female FSHD2 patients *vs.* female controls. CDP, cumulative distribution plot; ES, embryonic stem; FSHD2, facioscapulohumeral muscular dystrophy type 2; NPC, neural progenitor cell; WT, wild-type; XCI, X-chromosome inactivation.

confirmed *Pcdha* upregulation. Interestingly, we also observed increased antisense transcription at regions harboring alternate exons in *Smchd1*$^{-/-}$ cells (Figure 5A and Figure S2B, "−" strand).

We then investigated changes at the *Pcdh* locus at the level of chromatin using published epigenomic profiling data (Wang *et al.* 2018). In the WT clone, only one alternate (*Pcdha12*) and two C-type exons (*Pcdhac1* and *Pcdhac2*) were marked by the active H3K4me3 histone mark (Figure 5A) [note that in WT clones shown in Figure 5B, *Pcdha12*, *Pcdhac1*, and *Pcdhac3* did not show greater expression (FPKM) than other isoforms, as reads mapped to the constant exons were counted for all *Pcdhas*]. In *Smchd1*$^{-/-}$ cells, all variable exons became H3K4me3-enriched, coinciding with depletion of the repressive H3K27me3 histone mark and aberrant expression of all *Pcdha* isoforms (Figure 5, A and B), consistent with a previous report (Chen *et al.* 2015).

Transcription of *Pcdha* genes is regulated by *h*ypersensitivity *site 5-1* (HS5-1), an enhancer element located downstream of the last constant exon (Figure 5A) (Ribich *et al.* 2006; Kehayova *et al.* 2011). HS5-1 interacts with *Pcdha* promoters via long-range DNA looping mediated by two architectural factors, CTCF and cohesin (Guo *et al.* 2012; Monahan *et al.* 2012). We found that in *Smchd1*$^{-/-}$ mouse NPCs, activation of *Pcdha1-11* was associated with increased binding of not only CTCF [as previously reported (Chen *et al.* 2015)] but also RAD21, a cohesin subunit, to their respective promoters (Figure 5A and Figure S2B). We then examined *in situ* Hi-C data sets in WT and *Smchd1*$^{-/-}$ mouse cells (Wang *et al.* 2018) to determine if enhanced CTCF/cohesin binding is accompanied by altered 3D topological organization of this locus. Strikingly, chromatin interactions between *Pcdha1-12* promoters and the HS5-1 enhancer became more frequent in *Smchd1*$^{-/-}$ than those

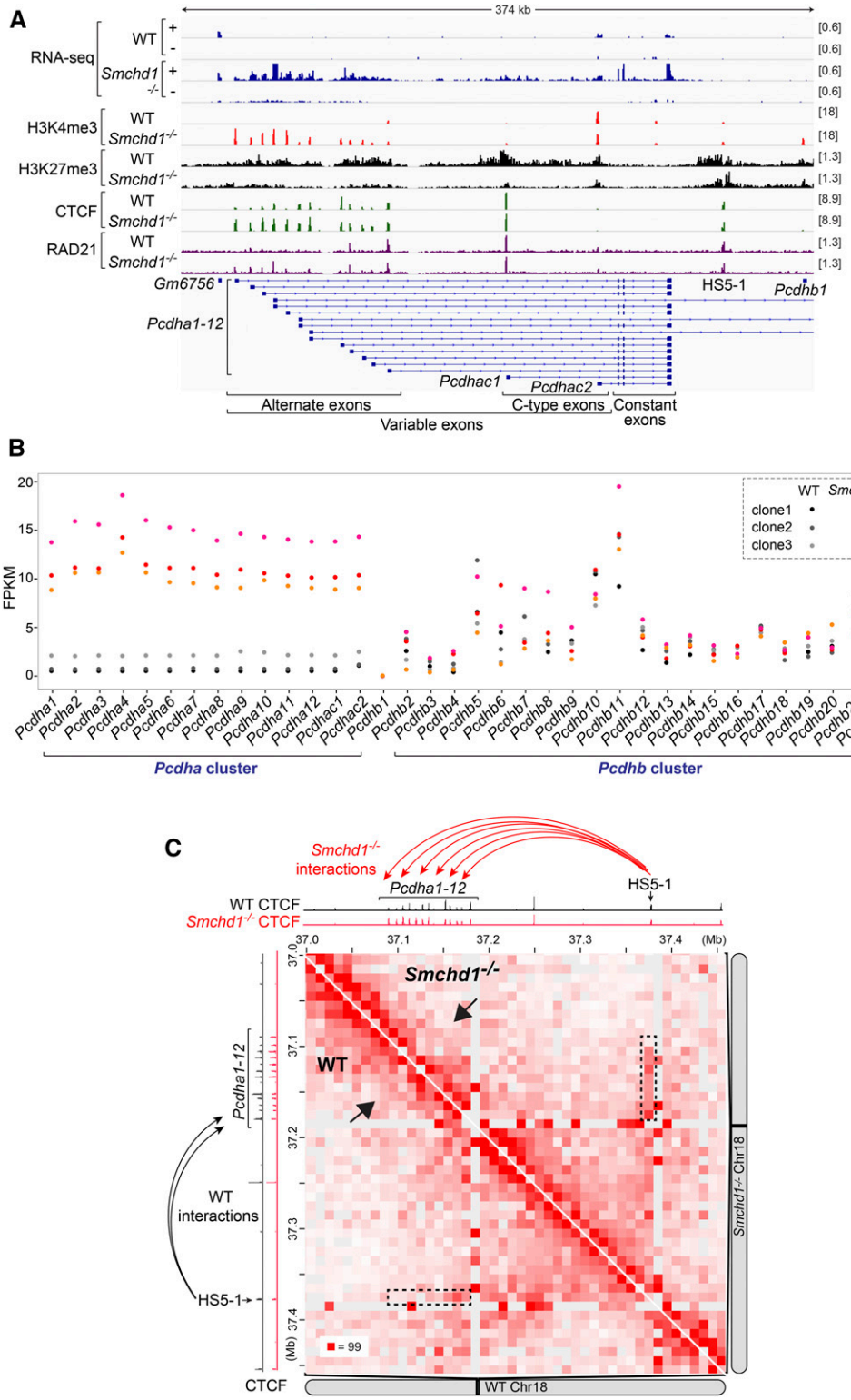

Figure 5 *Smchd1* ablation alters the expression, chromatin states, and three-dimensional organization of the *Pcdha* gene cluster in mice. (A) RNA-seq, H3K4me3, H3K27me3, CTCF, and RAD21 ChIP-seq (GSE99991) tracks at the *Pcdha* cluster in WT (clone1) and *Smchd1*$^{-/-}$ (clone1) female mouse NPCs, with scales indicated in each track. +, the plus strand. −, the minus strand. (B) Dot plots showing the FPKMs of the 14 *Pcdha* and 22 *Pcdhb* genes in WT ($n = 3$) and *Smcdh1*$^{-/-}$ ($n = 3$) mouse NPC clones. (C) Hi-C contact maps at 10-kb resolution at the *Pcdh*α cluster in WT (clone1, bottom) and *Smchd1*$^{-/-}$ (clone1, top) female mouse NPCs (GSE99991). Also shown are CTCF ChIP-seq tracks in WT (black) and *Smchd1*$^{-/-}$ (red) female mouse NPCs. ChIP-seq, chromatin immunoprecipitation-sequencing; Chr, chromosome; CTCF, CCCTC-binding factor; FPKM, fragments per kilobase of transcript per million mapped reads; NPC, neural progenitor cell; RNA-seq, RNA-sequencing; WT, wild-type.

in WT cells (Figure 5C, dashed rectangles), although the limited resolution of the Hi-C data sets did not allow us to pinpoint contacts between HS5-1 and each individual *Pcdha1-12* promoter. Moreover, increased CTCF/cohesin binding at the *Pcdha5* promoter in *Smchd1*$^{-/-}$ cells coincided with a strengthened border that appeared to separate *Pcdha1-12* into two small interacting domains (Figure 5C, arrows). Thus, our analyses revealed that SMCHD1 regulates not only the expression, but also the chromatin states and 3D organization, of the *Pcdha* gene cluster in mice.

Aberrant expression of PCDHA genes in arhinia and FSHD2 patients

Given effects on the mouse *Pcdha* locus, we asked if human *PCDH* clusters are affected by the arhinia and FSHD2-associated *SMCHD1* mutations. While the *PCDH* genes are predominantly expressed in the nervous system, clustered *Pcdh/PCDH* upregulation has been detected in nonneuronal lineages, such as in *Smchd1*$^{-/-}$ whole-mouse embryos (Gendrel *et al.* 2013; Mould *et al.* 2013), *Smchd1*$^{-/-}$ mouse embryonic fibroblasts (Leong *et al.* 2013), and FSHD2 human myogenic cells (Yao *et al.* 2014; Mason *et al.* 2017). With this in mind, we examined *PCDH* expression in RNA-seq data of LCLs from four females (Figure 1A) and six males (Figure S3A) with arhinia, with 10 unaffected individuals serving as controls. Interestingly, we observed upregulation of *PCDHA* genes in two arhinia patients (B1 and Y1) (Figure 6A and Table S2), but not in any of the controls. On the other hand, the *PCDHB* cluster was not expressed in LCLs even in normal cells (FPKM < 0.1), and the *PCDHG* cluster was not differentially expressed in patient *vs.* normal cells (Figure S3B).

Therefore, we focused on *PCDHA* and inspected strand-specific RNA-seq coverage tracks. We observed distinct patterns of *PCDHA* derepression in these two arhinia patients. In patient B1, most RNA-seq reads of the *PCDHA* genes originated from variable exons, but many reads were mapped to the intronic regions between alternate exons (Figure 6B, "+" strand) [note that in Figure 6A, B1 did not appear to be upregulated as strongly as what was shown in Figure 6B because only exonic reads were counted in the FPKM analysis). Furthermore, *PCDHA* derepression in B1 was associated with enhanced antisense transcription (Figure 6B, "−" strand), reminiscent of the pattern seen in *Smchd1*$^{-/-}$ mouse NPCs (Figure 5A). This distinct profile was detected in B1, but not in any other arhinia patients ($n = 9$) or controls ($n = 10$) (Figure 6B). Notably, the intronic and antisense *PCDHA* reads did not stem from artifacts of library construction and/or sequencing, as the RNA-seq of patient B1 at other loci exhibited characteristic exonic enrichment in the sense orientation (Figure S3C), and were sequenced to a depth similar to other patients/controls.

In patient Y1, *PCDHA* RNA-seq reads originated predominantly from the last constant exon (Figure 6B). All *PCDHA* isoforms were therefore counted as upregulated in the FPKM analysis (Figure 6A). We noted that patient A1, who carried the same missense mutation (p.Asn139His) as Y1, did not exhibit *PCDHA* upregulation (Figure 6B). These data imply that this *SMCHD1* mutation is not sufficient to cause misexpression of the *PCDHA* cluster; there are likely modifier genes that aid suppression of *PCDHA* in the presence of the *SMCHD1* missense mutation.

We also examined clustered *PCDH* expression in four FSHD2 patients carrying *SMCHD1* mutations using RNA-seq data of their muscle biopsies (Yao *et al.* 2014). Eight healthy individuals (controls), nine FSHD1 patients, and two FSHD2 patients without *SMCHD1* mutations were also analyzed (Yao *et al.* 2014). Expression of all three *PCDH* clusters was detected in muscle biopsies. In one FSHD2 patient (F14), we found upregulation of all *PCDHA* and three *PCDHB* isoforms (Figure 6C, Figure S4A, and Table S2), but not the *PCDHG* genes (Figure S4B). RNA-seq coverage profiles also revealed increased read density at the *PCDHA* loci in F14 (Figure 6D); however, we could not evaluate antisense transcription as the libraries were constructed using a non-strand-specific protocol. *PCDHA* upregulation was not detected in other FSHD1 and FSHD2 patients, suggesting an effect specific to this *SMCHD1* mutation and/or other factors unique to F14. *In vitro*-cultured myotubes from F14 also exhibited *PCDHA* upregulation (Figure S5), although there was considerable variation in the expression levels of *PCDHA* in control myotubes. Taken together, our observation of *PCDHA* upregulation in several arhinia and FSHD2 patients suggests that SMCHD1 may regulate this gene cluster in humans, as in mice. Genetic background and modifier loci can clearly also influence *PCDHA* expression when SMCHD1 activity is aberrant.

Smchd1 ablation causes aberrant regulation of Hox genes in mice

To identify additional classes of autosomal genes controlled by SMCHD1, we performed functional annotation clustering on autosomal genes differentially expressed in *Smchd1*$^{-/-}$ mouse NPCs (Tables S3 and S4) (Wang *et al.* 2018). Strikingly, among the upregulated autosomal genes ($n = 251$), we found homeobox genes, a group of transcription factors that control early embryonic development, to be one of the most highly enriched functional clusters (enrichment score = 5.4; $P = 2.6 \times 10^{-11}$), second only to the protocadherin genes (enrichment score = 6.39; $P = 3.9 \times 10^{-7}$) (Table S5). In contrast, no functional clusters in downregulated genes ($n = 82$) achieved statistical significance (Table S6).

Around 67% (10/15) of the homeobox genes derepressed in *Smchd1*$^{-/-}$ mouse NPCs are members of the *Hox* gene family, which controls the body plans in metazoans (Lewis 1978; Izpisúa-Belmonte *et al.* 1991; Duboule 2007). *Hox* genes, like the *Pcdh* genes, are clustered. There are four *Hox* clusters in vertebrates: *HoxA*, *HoxB*, *HoxC*, and *HoxD* (Duboule and Dolle 1989; Graham *et al.* 1989). The ordering of *Hox* genes within each cluster matches their unique spatiotemporal expression pattern during embryonic development, with genes at the 3′ end of the cluster being activated earlier and along the length of the animal ("anterior *Hox* genes"), and genes at the 5′ end being expressed later and in posterior structures ("posterior *Hox* genes") (Lewis 1978; Izpisúa-Belmonte *et al.* 1991; Duboule 2007). In three WT mouse NPC clones, we observed the same pattern of *Hox* expression, with only the anterior portion of *HoxA* (*Hoxa1-7*) being activated and the others remaining repressed (Figure 7A, black and gray bars), indicative of the rostral identity of these cells. While *Hoxa1-7* remained active in the absence of SMCHD1, all three *Smchd1*$^{-/-}$ clones exhibited aberrant *Hox* derepression (Figure 7A). Interestingly, in contrast to the

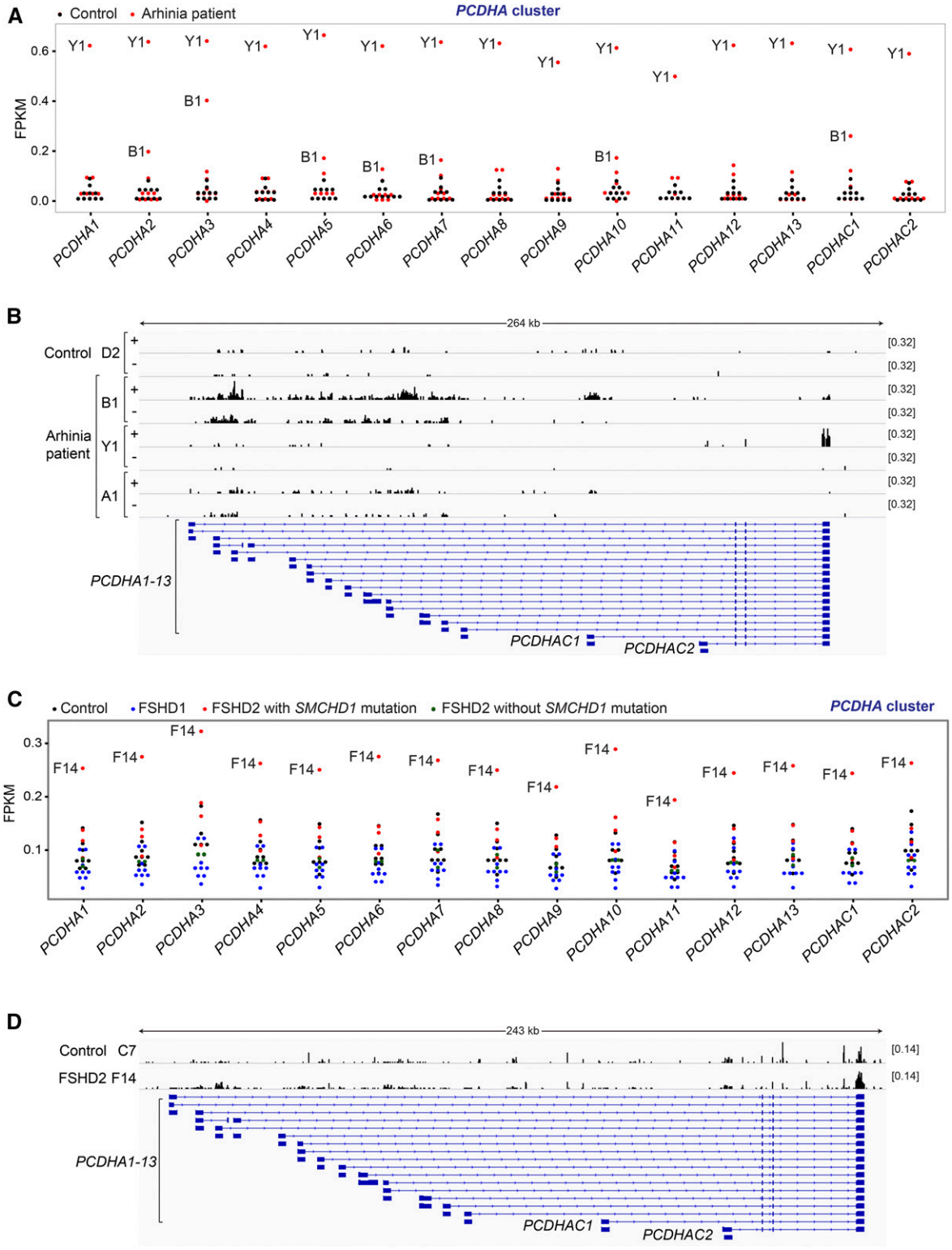

Figure 6 Dysregulation of the *PCDHA* gene cluster in arhinia and FSHD2 patients. (A) Dot plots showing the FPKMs of the 15 *PCDHA* genes in LCLs of 10 arhinia patients (red) and 10 controls (black). See Table S2 for the results of DESeq analyses, which similarly showed upregulation of *PCDHA* genes in patient Y1 and B1. (B) Strand-resolved RNA-seq coverage tracks at the *PCDHA* gene cluster of three arhinia patients (B1,Y1, and A1) and one control (D2). +, the plus strand. −, the minus strand. (C) Dot plots showing the FPKMs of the 14 *PCDHA* genes in muscle biopsies of nine FSHD1 patients (blue), four FSHD2 patients carrying SMCHD1 mutations (red), two FSHD2 patients without SMCHD1 mutations (green), and eight controls (black). See Table S2 for the results of DESeq analyses, which similarly showed upregulation of *PCDHA* genes in patient F14. (D) RNA-seq coverage tracks at the *PCDHA* gene cluster of one FSHD2 patients (F14) and one control (C7). +, the plus strand. −, the minus strand. FPKM, fragments per kilobase of transcript per million mapped reads; FSHD2, facioscapulohumeral muscular dystrophy type 2; LCL; lymphoblastoid cell line; RNA-seq, RNA-sequencing; SMCHD1, structural maintenance of chromosomes flexible hinge domain-containing 1.

uniform upregulation of the *Pcdha* cluster (Figure 5B), derepression of *Hox* genes was heterogeneous. Aberrant *Hox* activation appeared in all four paralogous clusters, but the number of activated genes varied not only between *Hox* clusters but also between different NPC clones (Figure 7A). Furthermore, we detected derepression not only of members of the *Hoxa1-7* paralogy groups, but also posterior *Hox* genes such as *Hox9-10*, indicative of caudal/posterior transformation.

Hox genes are regulated by Polycomb group proteins, a set of repressive histone-modifying complexes that control developmental genes (Schwartz and Pirrotta 2007; Soshnikova and Duboule 2009; Surface *et al.* 2010). Indeed, the derepressed *Hox* loci were accompanied by decreased occupancy of EZH2, the catalytic subunit of *P*olycomb *R*epressive *C*omplex 2 (PRC2), and its catalytic product, the H3K27me3 histone mark, in all four *Hox* clusters (Figure 7B, *HoxB*; Figure S6, *HoxA* and *HoxD*; and Figure S7A, *HoxC*). These derepressed genes were instead enriched by H3K4me3. Ablating *Smchd1* is known to influence the binding of CTCF and cohesin (Chen *et al.* 2015; Wang *et al.* 2018; Gdula *et al.* 2019), as exemplified by the clustered *Pcdha* locus (Figure 5A). Indeed, altered binding intensity of CTCF and RAD21 at the *Hox* loci was occasionally observed at some sites (Figure 7B, and Figures S6 and S7A), but globally they did not bind more strongly compared to what was observed at the *Pcdha1-11* region (Figure 5A). This difference might reflect different regulatory mechanisms at play at these loci and also varying degrees of derepression in *Smchd1*$^{-/-}$ cells.

The *Hox* clusters reside at the borders between topologically associated domains (TADs), megabase-sized chromatin structures that insulate interactions between loci from different domains (Dixon *et al.* 2012; Nora *et al.* 2012) or submegabase-scale TAD-like structures (subTADs). This unique positioning at TAD/subTAD boundaries contributes to sequential *Hox* activation (Dixon *et al.* 2012; Andrey *et al.* 2013; Berlivet *et al.* 2013; Darbellay and Duboule 2016). For instance, the *HoxB* cluster lies between two subTADs on mouse chromosome 11 (Figure 7C, dashed lines), with the boundary at the region between *Hoxb9* and *Hoxb13*. Intriguingly, we examined *in situ* Hi-C data sets in *Smchd1*$^{-/-}$ NPCs (Wang *et al.* 2018) and found altered 3D organization at this subTAD boundary. The inter-subTAD interactions became decreased when *Smchd1* was ablated (Figure 7C). To better visualize altered chromatin structures, we generated a differential Hi-C interaction map by dividing the WT by the *Smchd1*$^{-/-}$ map, which revealed more frequent inter-subTAD interactions in WT cells than in *Smchd1*$^{-/-}$ cells (Figure 7D, arrows). Altered inter-subTAD interactions were also observed for the boundary housing the *HoxC* cluster (between *Hoxc9* and *Hoxc13*) (Figure S7, B and C, arrows), but not for the boundary downstream to *HoxC* (Figure S7, B and C, arrow heads), indicating an effect specific to *Hox*-associated boundaries. As Polycomb complexes are known to promote formation of self-interacting domains of compacted chromatin ("Polycomb domains") (Eskeland *et al.* 2010; Bantignies *et al.* 2011; Schoenfelder *et al.* 2015; Kundu *et al.* 2017), the attenuated inter-subTAD interactions might be attributable to weakening of Polycomb domains that normally span TAD/subTAD boundaries and/or from altered CTCF/cohesin binding near these borders.

Taken together, these data demonstrate that SMCHD1 plays a critical role in the proper regulation of the *Hox* clusters in mice. Overall, the negative effects of *Smchd1* ablation on Polycomb recruitment and the positive effects on H3K4me3, CTCF, and cohesin enrichment mirror what have been observed on the Xi (Jansz *et al.* 2018a; Sakakibara *et al.* 2018; Wang *et al.* 2018; Gdula *et al.* 2019). The accompanying changes in *Hox* domain topology are also consistent with a role for SMCHD1 in organizing 3D chromosomal structures. Thus, SMCHD1 plays a vital role on the *X* chromosome and select loci on autosomes in the mouse.

HOX gene regulation is preserved in LCLs of arhinia patients and muscle biopsies in FSHD2 patients

A role for SMCHD1 in controlling the mouse *Hox* genes is intriguing. Congenital arhinia often meets the diagnostic criteria of Bosma arhinia microphthalmia syndrome (Bosma *et al.* 1981) and is accompanied by other craniofacial abnormalities, such as cleft lip/palate, low-set ears, anophthalmia or microophthalmia, uveal colomoma, and hypogonadotropic hypogonadism. These phenotypes likely represent a developmental defect in cranial placodes and/or neural crest cells (NCCs) (Gordon *et al.* 2017; Shaw *et al.* 2017). In light of the critical role of *Hox* genes in regulating the specification and migration of cranial NCCs during development [reviewed in Parker *et al.* (2018)], our finding suggests that *SMCHD1* mutations might cause arhinia and its associated craniofacial defects via dysregulation of the *Hox* genes. For instance, cranial NCCs derived from the anterior-most region of the neural tube, which normally lack *Hox* expression (Krumlauf 1993), may be susceptible to ectopic *Hox* expression when SMCHD1 is dysfunctional. The posterior transformation observed in *Smchd1*$^{-/-}$ mouse NPCs also supports speculation that rostral structures, such as derivatives of cranial NCCs, might be susceptible to phenotypic alteration associated with SMCHD1 dysfunction. With this in mind, we investigated *HOX* gene expression in the RNA-seq data of arhinia patients, noting that the data were from LCLs and not NCCs. We detected expression of *HOXB2-4*, *HOXB7*, and *HOXC4* in the LCLs of control individuals ($n = 10$) (Figure 8A, black dots). However, this expression pattern was unchanged in LCLs of arhinia patients ($n = 10$) (Figure 8A, red dots).

We then investigated *HOX* expression in FSHD2 patients using RNA-seq data from muscle biopsies ($n = 3$). The *HOX* expression pattern was the same in controls and FSHD2 patients (Figure 8B, red dots). Muscle biopsies from FSHD1 patients (Figure 8B, blue dots) and FSHD2 patients without *SMCHD1* mutations (Figure 8B, green dots) also exhibited similar *HOX* patterns. Together, we conclude that *SMCHD1* mutations in the heterozygous state do not alter *HOX*

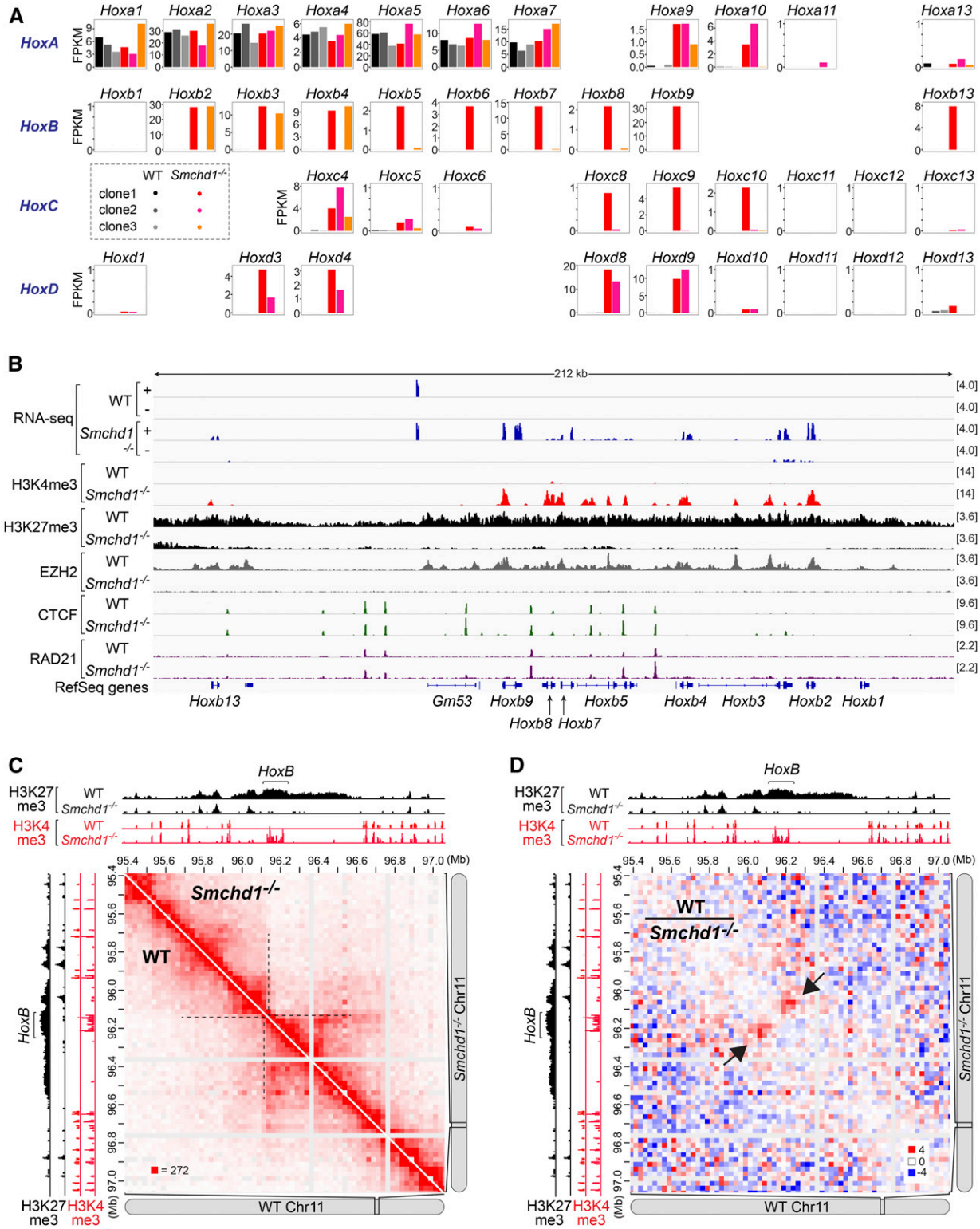

Figure 7 *Smchd1* ablation alters the expression, chromatin states, and three-dimensional organization of the *HoxB* gene cluster in mice. (A) Bar plots showing the FPKMs of all four clusters of *Hox* genes in WT ($n = 3$) and *Smcdh1*$^{-/-}$ ($n = 3$) mouse NPC clones. (B) RNA-seq, H3K4me3, H3K27me3, EZH2, CTCF, and RAD21 ChIP-seq (GSE99991) tracks at the *HoxB* cluster in WT (clone1) and *Smchd1*$^{-/-}$ (clone1) female mouse NPCs, with scales indicated in each track. +, the plus strand. −, the minus strand. (C) Hi-C contact maps at 25-kb resolution at the *HoxB* cluster in WT (clone1, bottom) and *Smchd1*$^{-/-}$ (clone1, top) female mouse NPCs (GSE99991). Also shown are H3K4me3 and H3K27me3 ChIP-seq tracks in WT and *Smchd1*$^{-/-}$ female mouse NPCs. (D) Differential Hi-C contact maps generated by dividing the WT with the *Smchd1*$^{-/-}$ contact map at 25-kb resolution at the *HoxB* cluster (GSE99991). ChIP-seq, chromatin immunoprecipitation-sequencing; CTCF, CCCTC-binding factor; FPKM, fragments per kilobase of transcript per million mapped reads; NPC, neural progenitor cell; RNA-seq, RNA-sequencing; WT, wild-type.

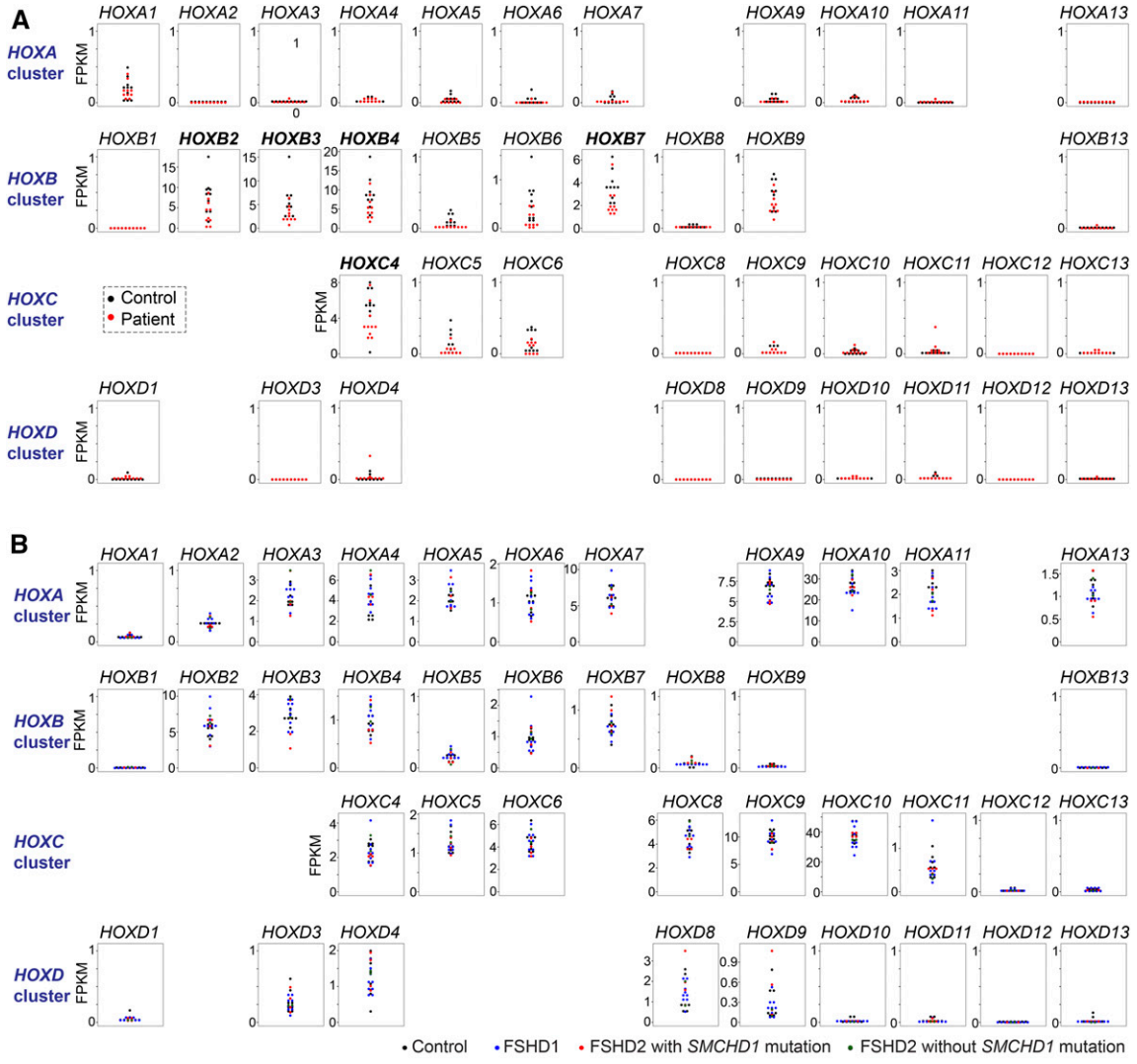

C

ID	Gene Name
Barhl2	BarH-like 2
Barx1	BarH-like homeobox 1
Nkx3-2	NK3 homeobox 2
Dlx2	distal-less homeobox 2
Hoxa10	homeobox A10
Hoxa9	homeobox A9
Hoxb2	homeobox B2
Hoxb3	homeobox B3
Hoxb4	homeobox B4
Hoxb9	homeobox B9
Hoxc4	homeobox C4
Hoxc5	homeobox C5
Hoxd3	homeobox D3
Hoxd9	homeobox D9
Vax2	ventral anterior homeobox 2

D

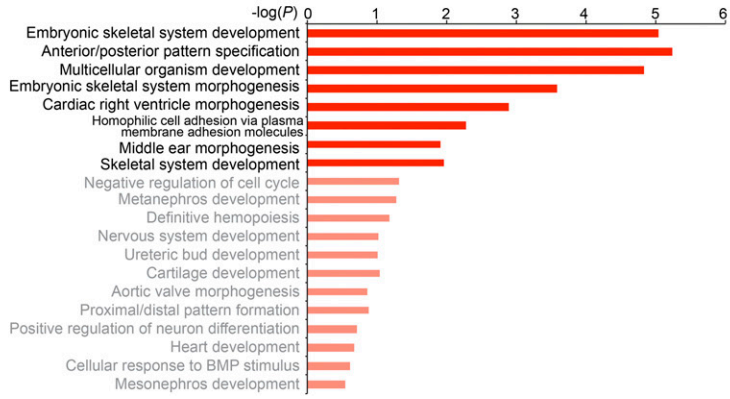

Figure 8 *HOX* genes are not dysregulated in LCLs of arhinia patients and muscle biopsies of FSHD2 patients. (A) Dot plots showing the FPKMs of the four clusters of *HOX* genes in LCLs of 10 arhinia patients (red) and 10 controls (black). (B) Dot plots showing the FPKMs of the four clusters of *HOX* genes in muscle biopsies of nine FSHD1 patients (blue), four FSHD2 patients carrying SMCHD1 mutations (red), two FSHD2 patients without SMCHD1 mutations (green), and eight controls (black).(C) A table listing other homeobox genes upregulated in *Smchd1*$^{-/-}$ mouse NPCs. (D) The top 20 list of the GO analysis of the 230 upregulated genes in *Smchd1*$^{-/-}$ mouse NPCs. GO terms that were not enriched with statistical significance were labeled with lighter colors. FPKM, fragments per kilobase of transcript per million mapped reads; FSHD2, facioscapulohumeral muscular dystrophy type 2; GO, gene ontology; ID, identifier; LCL; lymphoblastoid cell line; NPC, neural progenitor cell; SMCHD1, structural maintenance of chromosomes flexible hinge domain-containing 1.

expression in LCLs of arhinia patients and muscle biopsies of FSHD2 patients.

Derepression of genes involved in craniofacial development in Smchd1$^{-/-}$ mouse NPCs

Because it is not possible to study a homozygous SMCHD1 null in humans (see the *Introduction*), we turned again to the mouse to gain more insight into how the transcriptional program affected by SMCHD1 dysfunction might contribute to arhinia. We examined the function of other SMCHD1-regulated autosomal genes in mice. In addition to the *Hox* genes, *Smchd1* ablation led to upregulation of five non-*Hox* homeobox genes (Figure 8C). Among them was *D*istal-*l*ess homeob*x* (Dlx) 2, a family member of the *Dlx* gene family that plays a crucial role in the development of cranial NCCs and surface ectoderm derivatives, such as olfactory and otic placodes (Panganiban and Rubenstein 2002). Mice carrying homozygous mutations of *Dlx2* exhibit craniofacial defects, such as cleft palate (Qiu *et al.* 1995). Also identified was *V*entral *a*nterior homeob*x 2* (*Vax2*), a critical regulator of eye development, with its inactivation in mice being associated with incomplete closure of the optic fissure and eye coloboma (Barbieri *et al.* 2002). Thus, dysfunction of SMCHD1-regulated developmental regulators causes anomalies overlapping with arhinia-associated malformations. Consistent with these observations, GO analyses of SMCHD1-repressed autosomal genes revealed the enrichment for GO terms associated with embryonic development, pattern specification, and morphogenesis (Figure 8D) (Table S7). On the other hand, a GO analysis of downregulated autosomal genes in *Smchd1*$^{-/-}$ mouse NPCs did not reveal statistically significant enrichment of any GO terms (Table S8). We conclude that SMCHD1 deficiency in mouse NPCs leads to a dysregulated transcriptional program, where genes critical for craniofacial development become aberrantly expressed. These findings are consistent with the possibility that SMCHD1 may contribute to the pathogenesis of the craniofacial anomalies in arhinia through the dysregulation of homeobox genes.

Discussion

Here, we have integrated RNA-seq and epigenomic profiling data of *Smchd1*$^{-/-}$ mouse cells to understand the molecular pathogenesis of two human disorders associated with *SMCHD1* mutations: arhinia and FSHD2. Analysis of transcriptomic data from arhinia and FSHD2 patients demonstrate that the Xi chromosome remains dosage compensated in females. This finding is consistent with the absence of a sex bias in disease incidence or in clinical severity in patients with arhinia (Shaw *et al.* 2017 and N. Shaw, unpublished results). In fact, in FSHD multiplex families, females are more likely to be entirely asymptomatic or less symptomatic than male relatives (Zatz *et al.* 1995; Ricci *et al.* 1999, 2013; Tonini *et al.* 2004; Park *et al.* 2015) [however, this comparison may be confounded by the proposed protective effect of estrogen in FSHD, reviewed in Mul *et al.* (2018)]. Therefore, we conclude that XCI is not a contributor to the overall disease presentation and progression.

The absence of an effect on XCI may be somewhat surprising, but there are at least three possible explanations. First, all patients carry heterozygous mutations of *SMCHD1* and thus have some amount of functional protein. While the residual SMCHD1 activity may be insufficient to support proper craniofacial development (arhinia) and maintenance of muscle health (FSHD2), subtotal reduction of SMCHD1 function does not appear to impact XCI. This differential sensitivity may be due to the fact that, as shown by both immunofluorescence and epigenomic analysis of SMCHD1-binding sites, SMCHD1 is more concentrated on the Xi than anywhere else in the genome (Blewitt *et al.* 2008; Wang *et al.* 2018). The Xi's affinity for SMCHD1, as well as the multiple repressive mechanisms that synergize on the Xi, may render it less susceptible to subtotal reduction of normal SMCHD1 levels. Second, the missense *SMCHD1* mutations associated with arhinia may be hypomorphs rather than null mutations. Indeed, SMCHD1 abundance does not appear to be affected in cells (Shaw *et al.* 2017). If they are hypomorphic mutations or if the missense affects a region of SMCHD1 that is not critical for XCI, dosage compensation in females could be preserved. Finally, given that the patients have different genetic backgrounds, there could be modifier genes that ameliorate the effect of SMCHD1 dysfunction. It is also possible that there is a transient *X*–A imbalance in human females during a very early developmental window, as transient *X*-linked CpG hypomethylation has been observed in female *Smchd1*$^{MommeD1/+}$ mice at E8.5–10.5 (Blewitt *et al.* 2005, 2008). The patients could therefore represent survivors of delayed dosage compensation.

The resilience of *X*-linked genes to these mutations suggests that the necessity of intact SMCHD1 in silencing the Xi is different from susceptible loci on autosomes, such as *DUX4* (Lemmers *et al.* 2012). Our study demonstrates clear effects of SMCHD1 deficiency on a subset of autosomal gene clusters. SMCHD1 participates in establishing not only the expression pattern, but also the epigenetic states and chromatin architectures of five autosomal gene clusters—*Pcdha* (Figure 5) and all four clusters of *Hox* genes (Figure 7, Figures S6, and S7)—in mice. Our finding is consistent with a SMCHD1 ChIP-seq study showing association of SMCHD1 with the *Pcdh* and *Hox* clusters in mouse neural stem cells (Chen *et al.* 2015), and a concurrent study implicating SMCHD1 in *Hox* regulation (Jansz *et al.* 2018a). At the chromatin level, *Smchd1* ablation leads to enhanced binding of not only CTCF (Chen *et al.* 2015), but also cohesin at the *Pcdha* loci, coinciding with frequent enhancer–promoter contacts to facilitate transcription. At the *Hox* clusters, we observed erosion of H3K27me3 domains and decreased inter-subTAD interactions. These observations reinforce conclusions of previous work in which SMCHD1 was shown to weaken chromatin structures (TADs and compartments), enhance Polycomb recruitment, and repel the binding of canonical architectural proteins (Wang *et al.* 2018).

In support of a conserved role of human SMCHD1 in regulating *PCDH* and *HOX*, a previous study identified all three *PCDH* clusters, as well as the *HOXB* and *HOXD* clusters, to be CpG hypomethylated in peripheral blood mononuclear cells of non-FSHD-presenting female *SMCHD1* mutation carriers. This study also reported slight upregulation (~1.3–3-fold) of four *PCDHB* isoforms and one *HOX* gene in FSHD2 myoblast/myotube cultures, although the changes in *PCDHB* were also observed in FSHD1 cultures (Mason *et al.* 2017). Instead of *PCDHB*, we detected *PCDHA* dysregulation in the LCLs of two arhinia and the muscle biopsy of one FSHD2 patients. To our knowledge, *PCDHA* upregulation has not been reported in arhinia patients. Previous analysis of the same FSHD data sets reported *PCDHB2* as an FSHD2-specific upregulated gene (Yao *et al.* 2014), whereas our analysis suggests that *PCDHA/B* derepression may be more specific to one FSHD2 patient. While these data support a link between SMCHD1 dysfunction and *PCDHA* misregulation, not all arhinia/FSHD2 patients exhibit *PCDHA* upregulation, even when carrying an identical *SMCHD1* mutation (Figure 6B). The patterns of aberrant *PCDHA* upregulation observed in patients are also heterogeneous, sometimes accompanied by increased antisense transcription (Figure 6B). Together, these results suggest that regulation of the clustered *PCDH* genes is complex and may involve genetic or epigenetic modifiers that interact with SMCHD1. As the *PCDHA* cluster is a highly polymorphic region (Noonan *et al.* 2003) that is susceptible and tolerant to gene conversions (Miki *et al.* 2005) and deletions (Noonan *et al.* 2003) in humans, altered *PCDHA* expression may be related not to a change in SMCHD1 activity, but to one or more polymorphic SNPs in the *PCDHA* cluster in these patients. Another limitation of our study is that clustered *PCDHs* are lowly expressed in LCLs and myogenic cells, from which the patient RNA-seq data were generated, which likely explains why their upregulation does not reach statistical significance in DESeq analyses (Table S2). In light of the link between aberrant regulation of clustered *PCDH* genes and brain disorders (El Hajj *et al.* 2017), it may be relevant to examine *PCDH* expression in pertinent cell types (such as induced pluripotent stem cell-derived neurons) of these patients, and to evaluate potential neurological and psychiatric comorbidities (ClinialTrials.gov ID: NCT02032979).

However, we did not detect *HOX* gene dysregulation in arhinia and FSHD2 patients. While *HOX* genes may be more resilient to SMCHD1 dysfunction, it is also possible that *SMCHD1* mutations are associated with ectopic or precocious *HOX* expression in other cell types, such as NCCs, or during an earlier developmental window. Indeed, although *Hox* genes remain repressed in *Smchd1*$^{-/-}$ neural stem cells derived from the forebrain of mouse embryos (Chen *et al.* 2015), posterior homeotic transformation of the axial skeleton has recently been reported for these animals (Jansz *et al.* 2018a). Furthermore, premature or delayed *Hox* expression also causes phenotypes, even when the final expression pattern is normal (Gérard *et al.* 1997; Zakany *et al.* 1997; Kondo and Duboule 1999; Juan and Ruddle 2003). In addition to *Hox*, *Smchd1* ablation also leads to dysregulation of other homeobox genes critical for craniofacial development (Figure 8C). Additional work will be necessary to determine if these genes are dysregulated in the relevant cell types from patients, and their contribution to the pathogenesis of arhinia and FSHD2.

Acknowledgments

We thank S. Tapscott for providing genotypes of female FSHD2 patients; all members of the Lee laboratory for intellectual support; and M. Kuroda, S. Buratowski, and A. Gimelbrant for valuable advice during the thesis work of C.-Y.W. This work was supported by grants from the National Institutes of Health (NIH) (RO1 GM-090278 to J.T.L., K99 DE-026824 to H.B., and P01 GM-061354 to M.E.T.), the Intramural Research Program of the NIH, National Institute of Environmental Health Sciences (Z01 ES-103315 and 1SI2 ES-025429-01 to N.D.S.), the Rett Syndrome Research Trust (J.T.L.), and the Howard Hughes Medical Institute (J.T.L.).

Author contributions: C.-Y.W. and J.T.L. conceived the project. C.-Y.W. designed, performed, and interpreted the analyses. H.B., N.D.S., and M.E.T. provided the arhinia patient RNA-seq data sets. C.-Y.W., N.D.S., and J.T.L. wrote the paper with input from all authors. J.T.L. is a cofounder of, and a scientific advisor for, Translate Bio and Fulcrum Therapeutics.

Literature Cited

Anders, S., and W. Huber, 2010 Differential expression analysis for sequence count data. Genome Biol. 11: R106. https://doi.org/10.1186/gb-2010-11-10-r106

Andrey, G., T. Montavon, B. Mascrez, F. Gonzalez, D. Noordermeer *et al.*, 2013 A switch between topological domains underlies HoxD genes collinearity in mouse limbs. Science 340: 1234167. https://doi.org/10.1126/science.1234167

Balaton, B. P., and C. J. Brown, 2016 Escape artists of the X chromosome. Trends Genet. 32: 348–359. https://doi.org/10.1016/j.tig.2016.03.007

Balaton, B. P., A. M. Cotton, and C. J. Brown, 2015 Derivation of consensus inactivation status for X-linked genes from genome-wide studies. Biol. Sex Differ. 6: 35. https://doi.org/10.1186/s13293-015-0053-7

Bantignies, F., V. Roure, I. Comet, B. Leblanc, B. Schuettengruber *et al.*, 2011 Polycomb-dependent regulatory contacts between distant Hox loci in Drosophila. Cell 144: 214–226. https://doi.org/10.1016/j.cell.2010.12.026

Barbieri, A. M., V. Broccoli, P. Bovolenta, G. Alfano, A. Marchitiello *et al.*, 2002 Vax2 inactivation in mouse determines alteration of the eye dorsal-ventral axis, misrouting of the optic fibres and eye coloboma. Development 129: 805–813.

Berletch, J. B., F. Yang, J. Xu, L. Carrel, and C. M. Disteche, 2011 Genes that escape from X inactivation. Hum. Genet. 130: 237–245. https://doi.org/10.1007/s00439-011-1011-z

Berletch, J. B., W. Ma, F. Yang, J. Shendure, W. S. Noble *et al.*, 2015 Escape from X inactivation varies in mouse tissues. PLoS Genet. 11: e1005079. https://doi.org/10.1371/journal.pgen.1005079

Berlivet, S., D. Paquette, A. Dumouchel, D. Langlais, J. Dostie *et al.*, 2013 Clustering of tissue-specific sub-TADs accompanies the regulation of HoxA genes in developing limbs. PLoS Genet. 9: e1004018. https://doi.org/10.1371/journal.pgen.1004018

Blewitt, M. E., N. K. Vickaryous, S. J. Hemley, A. Ashe, T. J. Bruxner *et al.*, 2005 An N-ethyl-N-nitrosourea screen for genes involved in variegation in the mouse. Proc. Natl. Acad. Sci. USA 102: 7629–7634. https://doi.org/10.1073/pnas.0409375102

Blewitt, M. E., A. V. Gendrel, Z. Pang, D. B. Sparrow, N. Whitelaw *et al.*, 2008 SmcHD1, containing a structural-maintenance-of-chromosomes hinge domain, has a critical role in X inactivation. Nat. Genet. 40: 663–669. https://doi.org/10.1038/ng.142

Bosma, J. F., R. I. Henkin, R. L. Christiansen, and J. R. Herdt, 1981 Hypoplasia of the nose and eyes, hyposmia, hypogeusia, and hypogonadotrophic hypogonadism in two males. J. Craniofac. Genet. Dev. Biol. 1: 153–184.

Brideau, N. J., H. Coker, A. V. Gendrel, C. A. Siebert, K. Bezstarosti *et al.*, 2015 Independent mechanisms target SMCHD1 to trimethylated histone H3 lysine 9-modified chromatin and the inactive X chromosome. Mol. Cell. Biol. 35: 4053–4068. https://doi.org/10.1128/MCB.00432-15

Brockdorff, N., A. Ashworth, G. F. Kay, P. Cooper, S. Smith *et al.*, 1991 Conservation of position and exclusive expression of mouse Xist from the inactive X chromosome. Nature 351: 329–331. https://doi.org/10.1038/351329a0

Brown, C. J., A. Ballabio, J. L. Rupert, R. G. Lafreniere, M. Grompe *et al.*, 1991 A gene from the region of the human X inactivation centre is expressed exclusively from the inactive X chromosome. Nature 349: 38–44. https://doi.org/10.1038/349038a0

Calabrese, J. M., W. Sun, L. Song, J. W. Mugford, L. Williams *et al.*, 2012 Site-specific silencing of regulatory elements as a mechanism of X inactivation. Cell 151: 951–963. https://doi.org/10.1016/j.cell.2012.10.037

Carrette, L. L. G., C. Y. Wang, C. Wei, W. Press, W. Ma *et al.*, 2018 A mixed modality approach towards Xi reactivation for Rett syndrome and other X-linked disorders. Proc. Natl. Acad. Sci. USA 115: E668–E675. https://doi.org/10.1073/pnas.1715124115

Chen, K., J. Hu, D. L. Moore, R. Liu, S. A. Kessans *et al.*, 2015 Genome-wide binding and mechanistic analyses of Smchd1-mediated epigenetic regulation. Proc. Natl. Acad. Sci. USA 112: E3535–E3544. https://doi.org/10.1073/pnas.1504232112

Chen, K., R. C. Dobson, I. S. Lucet, S. N. Young, F. G. Pearce *et al.*, 2016 The epigenetic regulator Smchd1 contains a functional GHKL-type ATPase domain. Biochem. J. 473: 1733–1744. https://doi.org/10.1042/BCJ20160189

Chen, W. V., and T. Maniatis, 2013 Clustered protocadherins. Development 140: 3297–3302. https://doi.org/10.1242/dev.090621

Darbellay, F., and D. Duboule, 2016 Topological domains, metagenes, and the emergence of pleiotropic regulations at Hox loci. Curr. Top. Dev. Biol. 116: 299–314. https://doi.org/10.1016/bs.ctdb.2015.11.022

de Greef, J. C., Y. D. Krom, B. den Hamer, L. Snider, Y. Hiramuki *et al.*, 2018 Smchd1 haploinsufficiency exacerbates the phenotype of a transgenic FSHD1 mouse model. Hum. Mol. Genet. 27: 716–731. https://doi.org/10.1093/hmg/ddx437

Disteche, C. M., 2012 Dosage compensation of the sex chromosomes. Annu. Rev. Genet. 46: 537–560. https://doi.org/10.1146/annurev-genet-110711-155454

Dixon, J. R., S. Selvaraj, F. Yue, A. Kim, Y. Li *et al.*, 2012 Topological domains in mammalian genomes identified by analysis of chromatin interactions. Nature 485: 376–380. https://doi.org/10.1038/nature11082

Duboule, D., 2007 The rise and fall of Hox gene clusters. Development 134: 2549–2560. https://doi.org/10.1242/dev.001065

Duboule, D., and P. Dolle, 1989 The structural and functional organization of the murine HOX gene family resembles that of Drosophila homeotic genes. EMBO J. 8: 1497–1505. https://doi.org/10.1002/j.1460-2075.1989.tb03534.x

Durand, N. C., J. T. Robinson, M. S. Shamim, I. Machol, J. P. Mesirov *et al.*, 2016 Juicebox provides a visualization system for Hi-C contact maps with unlimited zoom. Cell Syst. 3: 99–101. https://doi.org/10.1016/j.cels.2015.07.012

El Hajj, N., M. Dittrich, and T. Haaf, 2017 Epigenetic dysregulation of protocadherins in human disease. Semin. Cell Dev. Biol. 69: 172–182. https://doi.org/10.1016/j.semcdb.2017.07.007

Eskeland, R., M. Leeb, G. R. Grimes, C. Kress, S. Boyle *et al.*, 2010 Ring1B compacts chromatin structure and represses gene expression independent of histone ubiquitination. Mol. Cell 38: 452–464. https://doi.org/10.1016/j.molcel.2010.02.032

Esumi, S., N. Kakazu, Y. Taguchi, T. Hirayama, A. Sasaki *et al.*, 2005 Monoallelic yet combinatorial expression of variable exons of the protocadherin-alpha gene cluster in single neurons. Nat. Genet. 37: 171–176. https://doi.org/10.1038/ng1500

Gdula, M. R., T. B. Nesterova, G. Pintacuda, J. Godwin, Y. Zhan *et al.*, 2019 The non-canonical SMC protein SmcHD1 antagonises TAD formation and compartmentalisation on the inactive X chromosome. Nat. Commun. 10: 30. https://doi.org/10.1038/s41467-018-07907-2

Gendrel, A. V., A. Apedaile, H. Coker, A. Termanis, I. Zvetkova *et al.*, 2012 Smchd1-dependent and -independent pathways determine developmental dynamics of CpG island methylation on the inactive X chromosome. Dev. Cell 23: 265–279. https://doi.org/10.1016/j.devcel.2012.06.011

Gendrel, A. V., Y. A. Tang, M. Suzuki, J. Godwin, T. B. Nesterova *et al.*, 2013 Epigenetic functions of smchd1 repress gene clusters on the inactive x chromosome and on autosomes. Mol. Cell. Biol. 33: 3150–3165. https://doi.org/10.1128/MCB.00145-13

Gendrel, A. V., M. Attia, C. J. Chen, P. Diabangouaya, N. Servant *et al.*, 2014 Developmental dynamics and disease potential of random monoallelic gene expression. Dev. Cell 28: 366–380. https://doi.org/10.1016/j.devcel.2014.01.016

Gérard, M., J. Zákány, and D. Duboule, 1997 Interspecies exchange of a Hoxd enhancer in vivo induces premature transcription and anterior shift of the sacrum. Dev. Biol. 190: 32–40. https://doi.org/10.1006/dbio.1997.8679

Gordon, C. T., S. Xue, G. Yigit, H. Filali, K. Chen *et al.*, 2017 De novo mutations in SMCHD1 cause Bosma arhinia microphthalmia syndrome and abrogate nasal development. Nat. Genet. 49: 249–255. https://doi.org/10.1038/ng.3765

Graham, A., N. Papalopulu, and R. Krumlauf, 1989 The murine and Drosophila homeobox gene complexes have common features of organization and expression. Cell 57: 367–378. https://doi.org/10.1016/0092-8674(89)90912-4

Guo, Y., K. Monahan, H. Wu, J. Gertz, K. E. Varley *et al.*, 2012 CTCF/cohesin-mediated DNA looping is required for protocadherin α promoter choice. Proc. Natl. Acad. Sci. USA 109: 21081–21086. https://doi.org/10.1073/pnas.1219280110

Gurzau, A. D., K. Chen, S. Xue, W. Dai, I. S. Lucet *et al.*, 2018 FSHD2- and BAMS-associated mutations confer opposing effects on SMCHD1 function. J. Biol. Chem. 293: 9841–9853. https://doi.org/10.1074/jbc.RA118.003104

Heinz, S., C. Benner, N. Spann, E. Bertolino, Y. C. Lin *et al.*, 2010 Simple combinations of lineage-determining transcription factors prime cis-regulatory elements required for macrophage and B cell identities. Mol. Cell 38: 576–589. https://doi.org/10.1016/j.molcel.2010.05.004

Huang da, W., B. T. Sherman, and R. A. Lempicki, 2009 Systematic and integrative analysis of large gene lists using DAVID bioinformatics resources. Nat. Protoc. 4: 44–57. https://doi.org/10.1038/nprot.2008.211

Izpisúa-Belmonte, J. C., H. Falkenstein, P. Dollé, A. Renucci, and D. Duboule, 1991 Murine genes related to the Drosophila AbdB homeotic genes are sequentially expressed during development of the posterior part of the body. EMBO J. 10: 2279–2289. https://doi.org/10.1002/j.1460-2075.1991.tb07764.x

Jansz, N., K. Chen, J. M. Murphy, and M. E. Blewitt, 2017 The epigenetic regulator SMCHD1 in development and disease. Trends Genet. 33: 233–243. https://doi.org/10.1016/j.tig.2017.01.007

Jansz, N., A. Keniry, M. Trussart, H. Bildsoe, T. Beck *et al.*, 2018a Smchd1 regulates long-range chromatin interactions on the inactive X chromosome and at Hox clusters. Nat. Struct. Mol. Biol. 25: 766–777. https://doi.org/10.1038/s41594-018-0111-z

Jansz, N., T. Nesterova, A. Keniry, M. Iminitoff, P. F. Hickey *et al.*, 2018b Smchd1 targeting to the inactive X is dependent on the Xist-HnrnpK-PRC1 pathway. Cell Rep. 25: 1912–1923.e9. https://doi.org/10.1016/j.celrep.2018.10.044

Jones, T. I., J. C. Chen, F. Rahimov, S. Homma, P. Arashiro *et al.*, 2012 Facioscapulohumeral muscular dystrophy family studies of DUX4 expression: evidence for disease modifiers and a quantitative model of pathogenesis. Hum. Mol. Genet. 21: 4419–4430. https://doi.org/10.1093/hmg/dds284

Juan, A. H., and F. H. Ruddle, 2003 Enhancer timing of Hox gene expression: deletion of the endogenous Hoxc8 early enhancer. Development 130: 4823–4834. https://doi.org/10.1242/dev.00672

Kehayova, P., K. Monahan, W. Chen, and T. Maniatis, 2011 Regulatory elements required for the activation and repression of the protocadherin-alpha gene cluster. Proc. Natl. Acad. Sci. USA 108: 17195–17200. https://doi.org/10.1073/pnas.1114357108

Kim, D., G. Pertea, C. Trapnell, H. Pimentel, R. Kelley *et al.*, 2013 TopHat2: accurate alignment of transcriptomes in the presence of insertions, deletions and gene fusions. Genome Biol. 14: R36. https://doi.org/10.1186/gb-2013-14-4-r36

Kondo, T., and D. Duboule, 1999 Breaking colinearity in the mouse HoxD complex. Cell 97: 407–417. https://doi.org/10.1016/S0092-8674(00)80749-7

Krumlauf, R., 1993 Hox genes and pattern formation in the branchial region of the vertebrate head. Trends Genet. 9: 106–112. https://doi.org/10.1016/0168-9525(93)90203-T

Kundu, S., F. Ji, H. Sunwoo, G. Jain, J. T. Lee *et al.*, 2017 Polycomb repressive complex 1 generates discrete compacted domains that change during differentiation. Mol. Cell **65:** 432–446.e5 [corrigenda: Mol. Cell 71: 191 (2018)]. https://doi.org/10.1016/j.molcel.2017.01.009

Lee, J. T., 2011 Gracefully ageing at 50, X-chromosome inactivation becomes a paradigm for RNA and chromatin control. Nat. Rev. Mol. Cell Biol. 12: 815–826. https://doi.org/10.1038/nrm3231

Lemmers, R. J., R. Tawil, L. M. Petek, J. Balog, G. J. Block *et al.*, 2012 Digenic inheritance of an SMCHD1 mutation and an FSHD-permissive D4Z4 allele causes facioscapulohumeral muscular dystrophy type 2. Nat. Genet. 44: 1370–1374. https://doi.org/10.1038/ng.2454

Lemmers, R. J., J. J. Goeman, P. J. van der Vliet, M. P. van Nieuwenhuizen, J. Balog *et al.*, 2015 Inter-individual differences in CpG methylation at D4Z4 correlate with clinical variability in FSHD1 and FSHD2. Hum. Mol. Genet. 24: 659–669. https://doi.org/10.1093/hmg/ddu486

Leong, H. S., K. Chen, Y. Hu, S. Lee, J. Corbin *et al.*, 2013 Epigenetic regulator Smchd1 functions as a tumor suppressor. Cancer Res. 73: 1591–1599. https://doi.org/10.1158/0008-5472.CAN-12-3019

Lewis, E. B., 1978 A gene complex controlling segmentation in Drosophila. Nature 276: 565–570. https://doi.org/10.1038/276565a0

Li, S. M., Z. Valo, J. Wang, H. Gao, C. W. Bowers *et al.*, 2012 Transcriptome-wide survey of mouse CNS-derived cells reveals monoallelic expression within novel gene families. PLoS One 7: e31751. https://doi.org/10.1371/journal.pone.0031751

Lopes, A. M., S. E. Arnold-Croop, A. Amorim, and L. Carrel, 2011 Clustered transcripts that escape X inactivation at mouse XqD. Mamm. Genome 22: 572–582. https://doi.org/10.1007/s00335-011-9350-6

Luijk, R., H. Wu, C. K. Ward-Caviness, E. Hannon, E. Carnero-Montoro *et al.*, 2018 Autosomal genetic variation is associated with DNA methylation in regions variably escaping X-chromosome inactivation. Nat. Commun. 9: 3738. https://doi.org/10.1038/s41467-018-05714-3

Marahrens, Y., B. Panning, J. Dausman, W. Strauss, and R. Jaenisch, 1997 Xist-deficient mice are defective in dosage compensation but not spermatogenesis. Genes Dev. 11: 156–166. https://doi.org/10.1101/gad.11.2.156

Marks, H., H. H. Kerstens, T. S. Barakat, E. Splinter, R. A. Dirks *et al.*, 2015 Dynamics of gene silencing during X inactivation using allele-specific RNA-seq. Genome Biol. 16: 149. [corrigenda: Genome Biol. 17: 22 (2016)] https://doi.org/10.1186/s13059-015-0698-x

Mason, A. G., R. C. Slieker, J. Balog, R. Lemmers, C. J. Wong *et al.*, 2017 SMCHD1 regulates a limited set of gene clusters on autosomal chromosomes. Skelet. Muscle 7: 12. https://doi.org/10.1186/s13395-017-0129-7

Miki, R., K. Hattori, Y. Taguchi, M. N. Tada, T. Isosaka *et al.*, 2005 Identification and characterization of coding single-nucleotide polymorphisms within human protocadherin-alpha and -beta gene clusters. Gene 349: 1–14. https://doi.org/10.1016/j.gene.2004.11.044

Mira-Bontenbal, H., and J. Gribnau, 2016 New Xist-interacting proteins in X–chromosome inactivation. Curr. Biol. 26: R338–R342. https://doi.org/10.1016/j.cub.2016.05.009

Monahan, K., N. D. Rudnick, P. D. Kehayova, F. Pauli, K. M. Newberry *et al.*, 2012 Role of CCCTC binding factor (CTCF) and cohesin in the generation of single-cell diversity of protocadherin-α gene expression. Proc. Natl. Acad. Sci. USA 109: 9125–9130. https://doi.org/10.1073/pnas.1205074109

Mould, A. W., Z. Pang, M. Pakusch, I. D. Tonks, M. Stark *et al.*, 2013 Smchd1 regulates a subset of autosomal genes subject to monoallelic expression in addition to being critical for X inactivation. Epigenetics Chromatin 6: 19. https://doi.org/10.1186/1756-8935-6-19

Mountoufaris, G., W. V. Chen, Y. Hirabayashi, S. O'Keeffe, M. Chevee *et al.*, 2017 Multicluster Pcdh diversity is required for mouse olfactory neural circuit assembly. Science 356: 411–414. https://doi.org/10.1126/science.aai8801

Mul, K., C. G. C. Horlings, N. C. Voermans, T. H. A. Schreuder, and B. G. M. van Engelen, 2018 Lifetime endogenous estrogen exposure and disease severity in female patients with facioscapulohumeral muscular dystrophy. Neuromuscul. Disord. 28: 508–511. https://doi.org/10.1016/j.nmd.2018.02.012

Noonan, J. P., J. Li, L. Nguyen, C. Caoile, M. Dickson *et al.*, 2003 Extensive linkage disequilibrium, a common 16.7-kilobase deletion, and evidence of balancing selection in the human protocadherin alpha cluster. Am. J. Hum. Genet. 72: 621–635. https://doi.org/10.1086/368060

Nora, E. P., B. R. Lajoie, E. G. Schulz, L. Giorgetti, I. Okamoto *et al.*, 2012 Spatial partitioning of the regulatory landscape of the X-inactivation centre. Nature 485: 381–385. https://doi.org/10.1038/nature11049

Nozawa, R. S., K. Nagao, K. T. Igami, S. Shibata, N. Shirai *et al.*, 2013 Human inactive X chromosome is compacted through a PRC2-independent SMCHD1-HBiX1 pathway. Nat. Struct. Mol. Biol. 20: 566–573. https://doi.org/10.1038/nsmb.2532

Panganiban, G., and J. L. Rubenstein, 2002 Developmental functions of the Distal-less/Dlx homeobox genes. Development 129: 4371–4386.

Park, H. J., J. M. Hong, J. H. Lee, H. S. Lee, H. Y. Shin *et al.*, 2015 Low D4Z4 copy number and gender difference in Korean patients with facioscapulohumeral muscular dystrophy type 1. Neuromuscul. Disord. 25: 859–864. https://doi.org/10.1016/j.nmd.2015.08.004

Parker, H. J., I. Pushel, and R. Krumlauf, 2018 Coupling the roles of Hox genes to regulatory networks patterning cranial neural crest. Dev. Biol. 444: S67–S78. https://doi.org/10.1016/j.ydbio.2018.03.016

Pinter, S. F., R. I. Sadreyev, E. Yildirim, Y. Jeon, T. K. Ohsumi *et al.*, 2012 Spreading of X chromosome inactivation via a hierarchy of defined Polycomb stations. Genome Res. 22: 1864–1876. https://doi.org/10.1101/gr.133751.111

Qiu, M., A. Bulfone, S. Martinez, J. J. Meneses, K. Shimamura *et al.*, 1995 Null mutation of Dlx-2 results in abnormal morphogenesis of proximal first and second branchial arch derivatives and abnormal differentiation in the forebrain. Genes Dev. 9: 2523–2538. https://doi.org/10.1101/gad.9.20.2523

Ribich, S., B. Tasic, and T. Maniatis, 2006 Identification of long-range regulatory elements in the protocadherin-alpha gene cluster. Proc. Natl. Acad. Sci. USA 103: 19719–19724. https://doi.org/10.1073/pnas.0609445104

Ricci, E., G. Galluzzi, G. Deidda, S. Cacurri, L. Colantoni *et al.*, 1999 Progress in the molecular diagnosis of facioscapulohumeral muscular dystrophy and correlation between the number of KpnI repeats at the 4q35 locus and clinical phenotype. Ann. Neurol. 45: 751–757. https://doi.org/10.1002/1531-8249(199906)45:6<751::AID-ANA9>3.0.CO;2-M

Ricci, G., I. Scionti, F. Sera, M. Govi, R. D'Amico *et al.*, 2013 Large scale genotype-phenotype analyses indicate that novel prognostic tools are required for families with facioscapulohumeral muscular dystrophy. Brain 136: 3408–3417. https://doi.org/10.1093/brain/awt226

Sacconi, S., R. J. Lemmers, J. Balog, P. J. van der Vliet, P. Lahaut *et al.*, 2013 The FSHD2 gene SMCHD1 is a modifier of disease severity in families affected by FSHD1. Am. J. Hum. Genet. 93: 744–751. https://doi.org/10.1016/j.ajhg.2013.08.004

Sakakibara, Y., K. Nagao, M. Blewitt, H. Sasaki, C. Obuse *et al.*, 2018 Role of SmcHD1 in establishment of epigenetic states required for the maintenance of the X-inactivated state in mice. Development 145: dev166462. https://doi.org/10.1242/dev.166462

Schoenfelder, S., R. Sugar, A. Dimond, B. M. Javierre, H. Armstrong *et al.*, 2015 Polycomb repressive complex PRC1 spatially constrains the mouse embryonic stem cell genome. Nat. Genet. 47: 1179–1186. https://doi.org/10.1038/ng.3393

Schwartz, Y. B., and V. Pirrotta, 2007 Polycomb silencing mechanisms and the management of genomic programmes. Nat. Rev. Genet. 8: 9–22. https://doi.org/10.1038/nrg1981

Shaw, N. D., H. Brand, Z. A. Kupchinsky, H. Bengani, L. Plummer *et al.*, 2017 SMCHD1 mutations associated with a rare muscular dystrophy can also cause isolated arhinia and Bosma arhinia microphthalmia syndrome. Nat. Genet. 49: 238–248 (erratum: Nat. Genet. 49: 969). https://doi.org/10.1038/ng.3743

Soshnikova, N., and D. Duboule, 2009 Epigenetic temporal control of mouse Hox genes in vivo. Science 324: 1320–1323. https://doi.org/10.1126/science.1171468

Splinter, E., E. de Wit, E. P. Nora, P. Klous, H. J. van de Werken *et al.*, 2011 The inactive X chromosome adopts a unique three-dimensional conformation that is dependent on Xist RNA. Genes Dev. 25: 1371–1383. https://doi.org/10.1101/gad.633311

Starmer, J., and T. Magnuson, 2009 A new model for random X chromosome inactivation. Development 136: 1–10. https://doi.org/10.1242/dev.025908

Sugathan, A., and D. J. Waxman, 2013 Genome-wide analysis of chromatin states reveals distinct mechanisms of sex-dependent gene regulation in male and female mouse liver. Mol. Cell. Biol. 33: 3594–3610. https://doi.org/10.1128/MCB.00280-13

Surface, L. E., S. R. Thornton, and L. A. Boyer, 2010 Polycomb group proteins set the stage for early lineage commitment. Cell Stem Cell 7: 288–298. https://doi.org/10.1016/j.stem.2010.08.004

Tasic, B., C. E. Nabholz, K. K. Baldwin, Y. Kim, E. H. Rueckert *et al.*, 2002 Promoter choice determines splice site selection in protocadherin alpha and gamma pre-mRNA splicing. Mol. Cell 10: 21–33. https://doi.org/10.1016/S1097-2765(02)00578-6

Tonini, M. M., M. R. Passos-Bueno, A. Cerqueira, S. R. Matioli, R. Pavanello *et al.*, 2004 Asymptomatic carriers and gender differences in facioscapulohumeral muscular dystrophy (FSHD). Neuromuscul. Disord. 14: 33–38. https://doi.org/10.1016/j.nmd.2003.07.001

Wang, C. Y., T. Jégu, H. P. Chu, H. J. Oh and J. T. Lee, 2018 SMCHD1 merges chromosome compartments and assists formation of super-structures on the inactive X. Cell 174: 406–421.e25. https://doi.org/10.1016/j.cell.2018.05.007

Wang, C. Y., D. Colognori, H. Sunwoo, D. Wang, and J. T. Lee, 2019 PRC1 collaborates with SMCHD1 to fold the X-chromosome and spread Xist RNA between chromosome compartments. Nat. Commun. 10: 2950. https://doi.org/10.1038/s41467-019-10755-3

Wang, X., H. Su, and A. Bradley, 2002 Molecular mechanisms governing Pcdh-gamma gene expression: evidence for a multiple promoter and cis-alternative splicing model. Genes Dev. 16: 1890–1905. https://doi.org/10.1101/gad.1004802

Wilkie, A. O., 2017 Many faces of SMCHD1. Nat. Genet. 49: 176–178. https://doi.org/10.1038/ng.3776

Wu, Q., and T. Maniatis, 1999 A striking organization of a large family of human neural cadherin-like cell adhesion genes. Cell 97: 779–790. https://doi.org/10.1016/S0092-8674(00)80789-8

Wu, Q., T. Zhang, J. F. Cheng, Y. Kim, J. Grimwood *et al.*, 2001 Comparative DNA sequence analysis of mouse and human protocadherin gene clusters. Genome Res. 11: 389–404. https://doi.org/10.1101/gr.167301

Wutz, A., 2011 Gene silencing in X-chromosome inactivation: advances in understanding facultative heterochromatin formation. Nat. Rev. Genet. 12: 542–553. https://doi.org/10.1038/nrg3035

Yagi, T., 2013 Genetic basis of neuronal individuality in the mammalian brain. J. Neurogenet. 27: 97–105. https://doi.org/10.3109/01677063.2013.801969

Yang, F., T. Babak, J. Shendure, and C. M. Disteche, 2010 Global survey of escape from X inactivation by RNA-sequencing in mouse. Genome Res. 20: 614–622. https://doi.org/10.1101/gr.103200.109

Yang, L., J. E. Kirby, H. Sunwoo, and J. T. Lee, 2016 Female mice lacking Xist RNA show partial dosage compensation and survive to term. Genes Dev. 30: 1747–1760. https://doi.org/10.1101/gad.281162.116

Yao, Z., L. Snider, J. Balog, R. J. Lemmers, S. M. Van Der Maarel *et al.*, 2014 DUX4-induced gene expression is the major molecular signature in FSHD skeletal muscle. Hum. Mol. Genet. 23: 5342–5352. https://doi.org/10.1093/hmg/ddu251

Zakany, J., M. Gerard, B. Favier, and D. Duboule, 1997 Deletion of a HoxD enhancer induces transcriptional heterochrony leading to transposition of the sacrum. EMBO J. 16: 4393–4402. https://doi.org/10.1093/emboj/16.14.4393

Zatz, M., S. K. Marie, M. R. Passos-Bueno, M. Vainzof, S. Campiotto *et al.*, 1995 High proportion of new mutations and possible anticipation in Brazilian facioscapulohumeral muscular dystrophy families. Am. J. Hum. Genet. 56: 99–105.

Zipursky, S. L., and J. R. Sanes, 2010 Chemoaffinity revisited: dscams, protocadherins, and neural circuit assembly. Cell 143: 343–353. https://doi.org/10.1016/j.cell.2010.10.009

Communicating editor: J. Schimenti